DESIGN AND ANALYSIS OF PATCH ANTENNA WITH TAPERED MATCHING SECTION FOR WLAN / WiMAX APPLICATIONS

THESIS SUBMITTED IN PARTIAL FULFILLMENT OF THE REQUIREMENT FOR THE DEGREE OF

MASTER OF TECHNOLOGY
IN
VLSI DESIGN AND MICROELECTRONICS TECHNOLOGY

THESIS SUBMITTED BY

PRITHIS SEN

University Registration No: 133984 of 2015-2016

Exam Roll No: M6VLS19019

Class Roll No: 001510713004

UNDER THE GUIDANCE OF

PROFESSOR BHASKAR GUPTA

DEPARTMENT OF ELECTRONICS AND TELE-COMMUNICATION ENGINEERING

JADAVPUR UNIVERSITY

KOLKATA – 700032

INDIA

FACULTY OF ENGINEERING AND TECHNOLOGY
ELECTRONICS AND TELECOMMUNICATION ENGINEERING
JADAVPUR UNIVERSITY

CERTIFICATE OF RECOMMENDATION

This is to certify that the thesis entitled "**DESIGN AND ANALYSIS OF PATCH ANTENNA WITH TAPERED MATCHING SECTION FOR WLAN / WiMAX APPLICATIONS**" has been carried out by **PRITHIS SEN** (***University Registration No: 133984 of 2015-2016***) under my guidance and supervision and be accepted in partial fulfilment of the requirement for awarding the degree of "**MASTER OF TECHNOLOGY in VLSI DESIGN AND MICROELECTRONICS TECHNOLOGY**". The research results presented in this thesis have not been included in any other paper submitted for the award of any degree to any other Institute or University

---

PROFESSOR BHASKAR GUPTA

THESIS SUPERVISOR

DEPT. OF ELECTRONICS AND TELECOMMUNICATION ENGINEERING
JADAVPUR UNIVERSITY
KOLKATA 700032

PROF. SHELI SINHA CHAUDHURI

HEAD OF THE DEPARTMENT

DEPT. OF ELECTRONICS AND TELECOMMUNICATION ENGINEERING

JADAVPUR UNIVERSITY
KOLKATA 700032

PROF. CHIRANJIB BHATTACHARJEE

DEAN

FACULTY OF ENGINEERING AND TECHNOLOGY

JADAVPUR UNIVERSITY
KOLKATA 700032

FACULTY OF ENGINEERING AND TECHNOLOGY
ELECTRONICS AND TELECOMMUNICATION ENGINEERING

JADAVPUR UNIVERSITY

CERTIFICATE OF APPROVAL#

The foregoing THESIS is hereby approved as a creditable study of an Engineering Subject carried out and presented in a manner of satisfactory to warrant its acceptance as a pre-requisite to the DEGREE for which it has been submitted. It is to be understood that by this approval, the undersigned do not necessarily endorse or approve any statement made, opinion expressed or conclusion drawn therein but approve the THESIS only for the purpose for which it has been submitted.

Committee on final examination
for the evaluation of the Thesis

_____
(Signature of the Supervisor)

_____
(Signature of the Examiner)

only in case the thesis is approved.

FACULTY OF ENGINEERING AND TECHNOLOGY
ELECTRONICS AND TELECOMMUNICATION ENGINEERING
JADAVPUR UNIVERSITY

DECLARATION OF ORIGINALITY AND COMPLIANCE OF ACADEMIC ETHICS

I hereby declare that this thesis contains literature survey and original research work done by the undersigned candidate, as a part of his degree of "**MASTER OF TECHNOLIGY in VLSI DESIGN AND MICROELECTRONICS TECHNOLOGY".** All information in this document has been obtained and presented in accordance with academic rules and ethical conduct. I also declare that as required by these rules and conduct, I have fully cited and referenced all materials and results that are not original to this work.

Thesis Title

DESIGN AND ANALYSIS OF PATCH ANTENNA WITH TAPERED MATCHING SECTION FOR WLAN / WiMAX APPLICATIONS

PRITHIS SEN

University Registration No: 133984 of 2015-2016

Exam Roll No: M6VLS19019

Class Roll No: 001510703004

DEPT. OF ELECTRONICS AND TELECOMMUNICATION ENGINEERING

JADAVPUR UNIVERSITY

KOLKATA – 700032

INDIA

Date: _____ _____

(PRITHIS SEN)

ACKNOWLEDGEMENT

Firstly, I wish to take this opportunity to thank my Master's supervisor **Professor Bhaskar Gupta** and acknowledge the deep impact he has had in cultivating within me the interest and curiosity that I have developed towards the theory and applications of Electromagnetism of which Microwave Engineering is but a small part. His patience, the immense knowledge he shares with us and the relationship he has with all his students clearly brings out the best in them. I am very thankful that I have been able to do my Master's thesis under the guidance of such an able and well established professor.

I would like to thank **Professor Bhaskar Gupta** for all his comments and discussions which have very often helped clear many of my doubts and helped me look at things from a different perspective. I also wish to express my gratitude to the previous head of the department, **Prof. Palaniandavar Venkateswaran** and the current head of the department **Prof. Sheli Sinha Chaudhuri** for always extending a helping hand whenever needed and giving me the opportunity of attending conferences where I could bring myself up to speed with the latest research in the fields of Electromagnetics currently happing worldwide.

This thesis would not have been complete without the help and co operation of all my seniors of JU Microwave Lab who took the time and effort to help me immensely with all my fabrications and indulge in very knowledgeable discourse which helped me learn a plethora of things regarding my subject that I was previously unaware of.

Lastly, but most importantly, I would like to thank my father and mother for encouraging me to pursue the subject I love and for their constant and unwavering faith in my abilities. Without their support, I would definitely not be where I am today.

Date: _____ _____

(PRITHIS SEN)

CONTENTS

CHAPTER 3

CHAPTER 4

Chapter 1

1. INTRODUCTION:

Antenna is one of the critical components in any wireless communication system. The word ‘antenna’ is derived from Latin word ‘antemna.’ Since the first demonstration of wireless technology by Heinrich Hertz and its first application in practical radio communication by Guglielmo Marconi, the antenna has been a key building block in the construction of every wireless communication system. IEEE defines an antenna as “a part of a transmitting or receiving system that is designed to radiate or receive electromagnetic waves.”

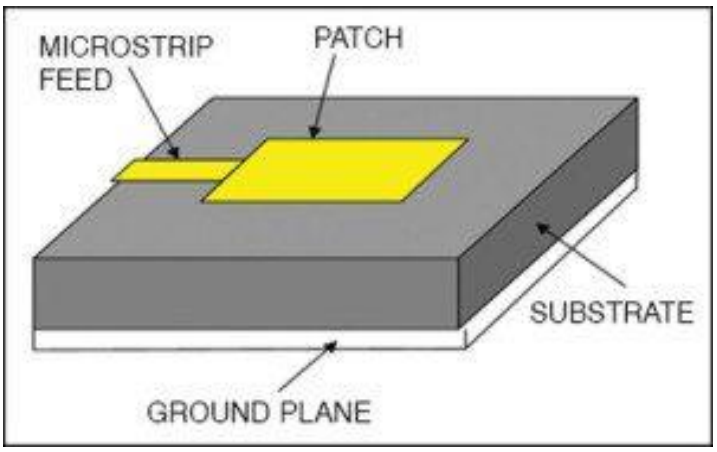

Fig. 1: Physical geometry of microstrip antenna

1.1. CLASSIFICATION:

Antennae could be broadly classified as wire antennae, aperture antennae, printed antennae, array antennae, reflector antennae and lens antenna.

1.1.1. APERTURE ANTENNA:

These antennae are in the form of a slot or aperture in a metal plate and commonly used at higher frequencies (3-30 GHz). Typical examples are slotted waveguide antennae and horn antennae. These antennae are very useful for aircraft and spacecraft applications, because they can be conveniently flush mounted on the surface of the aircraft or spacecraft. In practice, these antennae are covered with a dielectric material to protect them from hazardous environmental conditions.

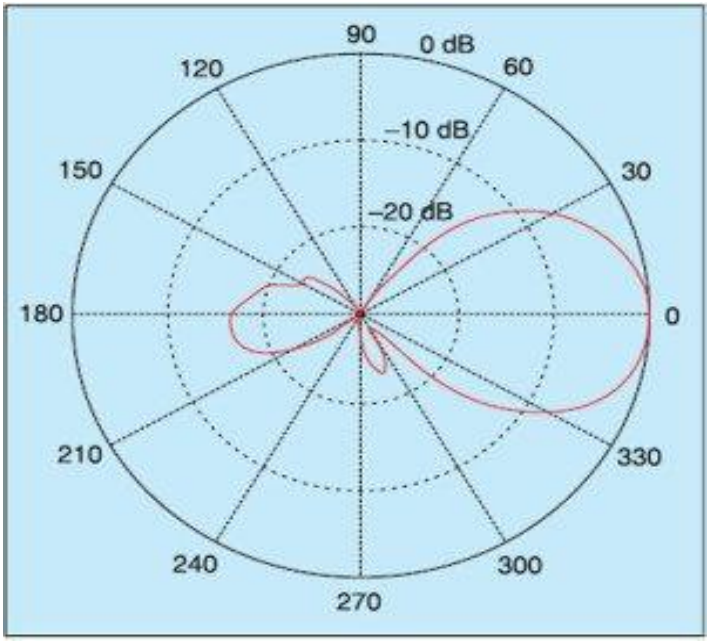

Fig. 2: Typical radiation pattern of microstrip antenna

1.1.2. PRINTED ANTENNA:

By definition, a printed antenna is one that is fabricated using standard photolithography technique. The most common version of printed antenna is microstrip antenna, which consists of a metallic patch above a ground plane. The shape and size of patch determine the frequency of operation of the antenna and its performance.

These antennae are more popular because of their low cost and ease of fabrication, and easy integration with circuit components. Printed

antennae are inexpensive to fabricate using modern printed circuit technology, and are conformal to planar and non-planar surfaces. These antennae can be easily mounted on the surface of aircrafts, spacecrafts, satellites, missiles and even on handheld mobile devices.

1.1.3. ARRAY ANTENNA:

In an array antenna, several radiators separated from each other are geometrically arranged to give desired radiation characteristics that are not possible to achieve with a single independent radiating element. The arrangement of array elements is such that radiation from individual elements adds up to give the maximum radiation in a particular direction or directions, and minimum radiation in other directions. In practice, individual radiators are arranged in linear or planar grid depending on the application.

1.1.4. REFLECTOR ANTENNA:

These antennae are specifically used in applications requiring communication over long distances, such as outer space exploration and satellite communication. They are built with large diameters in order to achieve the high gain required to transmit or receive signals over very long distances. The reflector antenna usually uses a smaller antenna as the feed.

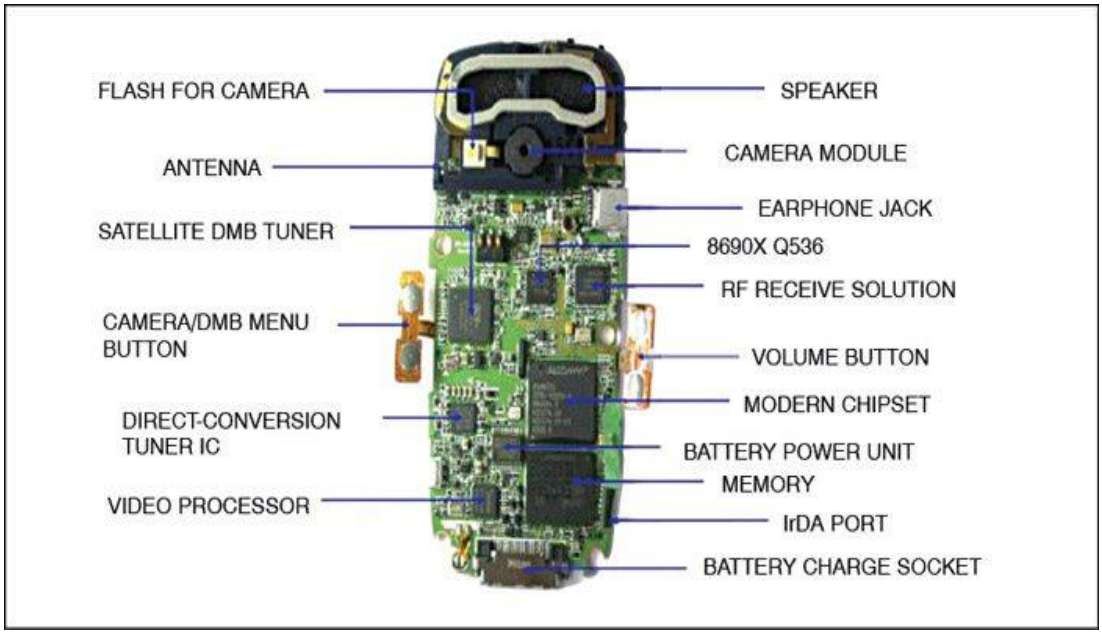

Fig. 3: Packaging detail inside a mobile handset with antenna

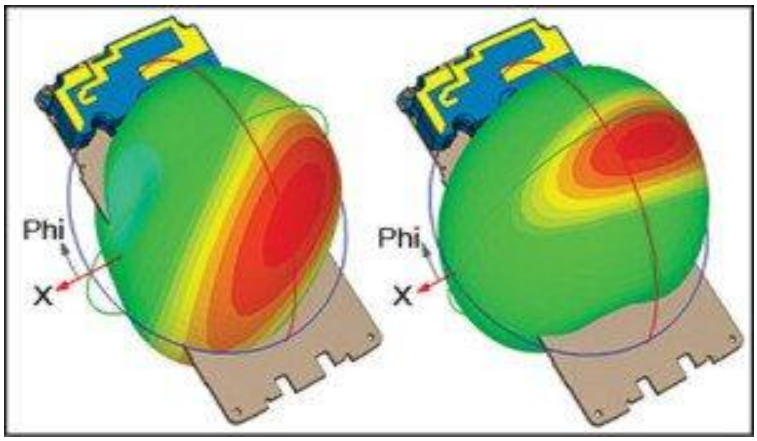

Fig. 4: GSM antenna radiation pattern for a cellphone

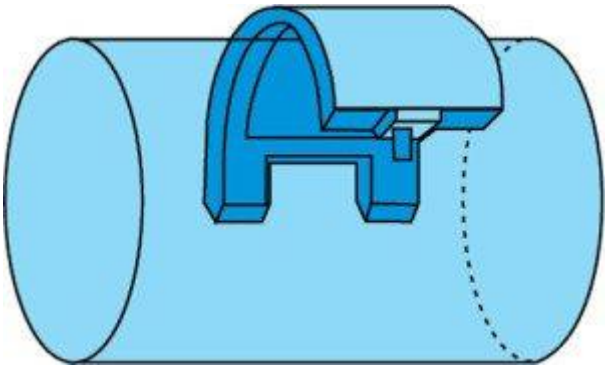

Fig. 5: Flexible microstrip applicator for hyperthermia medicinal applications

1.1.5. LENS ANTENNA:

In these antennae, lenses are used to collimate the incident divergent energy to prevent it from spreading in undesired directions. By choosing the appropriate material and setting the geometrical configuration of lenses, they can transform various forms of divergent energy into plane waves. Lens antennae are classified according to the material from which they are constructed or their geometrical shapes.

1.2. MICROSTRIP ANTENNA: THE MOST COMMON PRINTED ANTENNA:

Microstrip antenna is one of the most popular types of printed antenna. It plays a very significant role in today's world of wireless communication systems. Microstrip antennae are very simple in construction using a conventional microstrip fabrication technique. Microstrip patch antenna consists of a radiating patch on one side of a dielectric substrate (FR4) that has a ground plane (Cu) on the other side as shown in Fig. 1.

The patch is generally made up of a conducting material such as copper or gold and can take any possible shape like rectangular, circular, triangular, elliptical or some other common shape. The radiating patch and the feed lines are usually photo-etched on the dielectric substrate.

TABLE II
Comparison of Various Types of Microstrip Antennae

Characteristics	Microstrip patch antenna	Microstrip slot/ travelling-wave antenna	Printed dipole antenna
Profile	Thin	Thin	Thin
Fabrication	Very easy	Easy	Easy
Polarisation	Both linear and circular	Both linear and circular	Linear
Dual-frequency operation	Possible	Possible	Possible
Shape flexibility	Any shape	Mostly rectangular and circular shape	Rectangular and triangular
Spurious radiation	Exists	Exists	Exists
Bandwidth	2-50 per cent (resonant frequency)	5-30 per cent (resonant frequency)	30 per cent (resonant frequency)

Microstrip patch antennae radiate primarily because of the fringing fields between the patch edge and the ground plane. For good antenna performance, a thick dielectric substrate having a low dielectric constant (<6) is desirable since it provides higher efficiency, larger bandwidth and better radiation. However, such a configuration leads to a larger antenna size.

In order to design a compact microstrip patch antenna, a substrate with a higher dielectric constant (<12) must be used, which results in lower efficiency and narrower bandwidth. Hence a compromise must be reached between antenna dimensions and antenna performance. Excitation guides the electromagnetic energy source to the patch, generating negative charges around the feed point and positive charges on the other part of the patch. This difference in charges creates electric fields in the antenna that are responsible for radiations from the patch antenna.

Three types of electromagnetic waves are radiated. The first part is radiated into space, which is ‘useful’ radiation. The second part is diffracted

waves, which are reflected back into space between the patch and the ground plane, contributing to the actual power transmission. The last part of the wave remains trapped in the dielectric substrate due to total reflection at the air-dielectric separation surface. The waves trapped in the substrate are generally undesirable.

Different types of antennae have many different shapes and dimensions. Microstrip antennae can be classified into four subtypes: microstrip patch antennae, microstrip dipoles, printed slot antennae and microstrip travelling-wave antennae.

1.3. POLARISATION AND RADIATION OF MICROSTRIP ANTENNA:

The polarisation of an antenna is determined by the wave radiated in a given direction that is identical to the direction of the electric field. The instantaneous electric field vector traces a figure in time. This figure is usually an ellipse that has special cases. If the path of the electric field vector follows a line, the antenna is said to be linearly polarised. If the electric field vector rotates in a circle, it is called circularly polarised. To characterise the polarisation, axial ratio is used. It is defined by the following relationship:

$$T = \frac{\text{Large diameter of the ellipse}}{\text{Small diameter of the ellipse}}$$

Polarisation is said to be linear if $T \rightarrow \infty$ or $T = 0$, and circular if $T = 1$.

There are two sub-types of linear polarisation: Vertical polarisation and horizontal polarisation. When ‘E’ field vector of the EM wave is perpendicular to the earth, the EM wave is said to be vertically polarised. When

‘E’ field vector of the EM wave is parallel to the earth, the EM wave is said to be horizontally polarised.

The radiation pattern is a graphical depiction of the relative field strength transmitted from or received by the antenna. Antenna radiation patterns are taken at one frequency, one polarisation and one plane cut. Patterns are usually presented in polar or rectilinear form with a dB strength scale. These are normalised to the maximum graph value of 0 dB and directivity is given for the antenna. This means that if side-lobe level from the radiation pattern were down -13 dB, and directivity of the antenna was 4 dB, side-lobe gain would be -9 dB.

2. APPLICATION OF MICROSTRIP ANTENNA:

Communication-based applications. Microstrip patch antenna finds several applications in wireless communication. For example, satellite communication requires circularly polarised radiation patterns, which can be realised using either square or circular patch microstrip antenna. In global positioning satellite (GPS) systems, circularly polarised microstrip antennae are used. They are very compact in size and quite expensive due to their positioning.

Microstrip antennae are also used in the fields of RFID (radio frequency identification), mobile communication and healthcare. Basically, an RFID system consists of a tag and a reader. Generally, it uses frequencies between 30 Hz and 5.8 GHz.

In telemedicine application, microstrip antennae operate at 2.45 GHz. Wearable microstrip antennae are suitable for wireless body area network. An antenna having gain of 6.7 dB and front-to-back ratio of 11.7 dB, and resonating at 2.45 GHz is suitable for telemedicine applications.

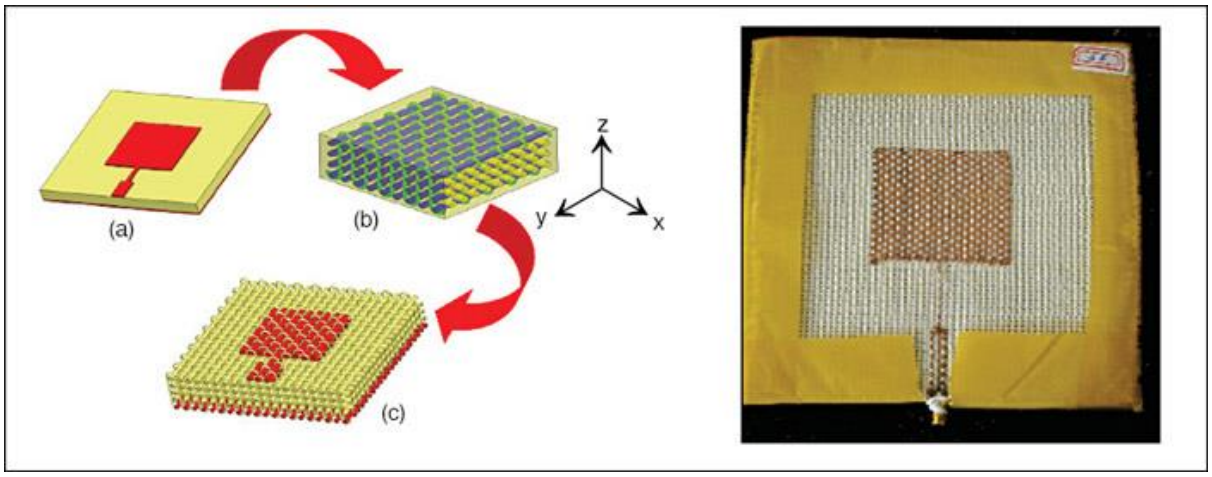

Fig. 6: Geometry of textile antenna

The IEEE 802.16 standard is known as WiMax (worldwide interoperability for microwave access). It can reach up to 48km (30-mile) radius with data rate of 70 Mbps. Microstrip antennae can resonate at more than one frequency. Therefore these can be used in WiMax-based communication equipment.

Some communication-based applications of microstrip patch antennae are radio altimeters, command and control systems, remote sensing and environmental instrumentation, feed elements in complex antennae, satellite navigation receivers, mobile radio, integrated antennae, biomedical radiators and intruder alarms, Doppler and other radars, and satellite communication and direct broadcast services.

2.1. MOBILE COMMUNICATION:

Mobile communication requires small, low-cost, low-profile antennae. In some mobile handsets, semiconductor-based diodes or detectors are used as antennae. They are much like p-n diode photo-detectors but work at microwave frequency. Many times omnidirectional antenna is used in mobile phones. There are different kinds of antennae like planar inverted-F antenna, folded inverted conformal antenna and mono pole. Also retractable whip antenna is commonly used in handsets.

The phone is subdivided into roughly 60 components, each consisting of hundreds or even thousands of individual facets. The internal structure of a mobile handset is shown in Fig. 3.

2.2. MEDICAL APPLICATION:

In the treatment of malignant tumours, microwave energy is said to be the most effective way of inducing hyperthermia. The radiator to be used for this purpose should be light-weight, easy to handle and rugged. Only a patch radiator fulfils these requirements.

The initial designs of microstrip radiators for inducing hyperthermia were based on printed dipoles and annular rings that were designed on S-band (2-4 GHz). Later on the design was based on a circular microstrip disk at L-band (1-2 GHz). Two coupled microstrip lines with a flexible separation are used to measure temperature inside the human body. Fig. 5 shows a flexible patch applicator that operates at 430 MHz.

2.3. TEXTILE ANTENNA: RECENT RESEARCH:

There are some applications at present where antennae are used to continuously monitor biometric data of the human body. In order to do this,

they need to be so close to the human body all the time that they can continuously monitor the biometric data and send the information to the outside world. If the antenna is hard, it cannot be kept always attached with the human body. An antenna made of textile material will not harm the human body and can be worn for extended periods. Wearable antennae will find use in healthcare, recreation, fire-fighting, etc.

Textile materials are increasingly being used for development of flexible wearable systems due to the recent miniaturisation of wireless devices. For flexible antennae, textile materials form interesting substrates, because fabric antennae can be easily integrated into clothes.

In this special type of patch antenna, the radiating patch and the ground plane are made up of conductive textile material. The substrate too is a textile material with specific dielectric constant. As everything is made up of textile material, it is called textile antenna.

Textile antennae are still under testing, so they are rarely in focus.

Chapter 2

1. INTRODUCTION:

Transmission line theory bridges the gap between field analysis and basic circuit theory and therefore is of significant importance in the analysis of microwave circuits and devices. As we will see, the phenomenon of wave propagation on transmission lines can be approached from an extension of circuit theory or from a specialization of Maxwell's equations; we shall present both viewpoints and show how this wave propagation is described by equations very similar to those used in previous chapter for plane wave propagation.

One of the early milestones in microwave engineering was the development of waveguide and other transmission lines for the low-loss transmission of power at high frequencies. Although Heaviside considered the possibility of propagation of electromagnetic waves inside a closed hollow tube in 1893, he rejected the idea because he believed that two conductors were necessary for the transfer of electromagnetic energy [1]. In 1897, Lord Rayleigh (John William Strutt) mathematically proved that wave propagation in waveguides was possible for both circular and rectangular cross sections [2]. Rayleigh also noted the infinite set of waveguide modes of the TE and TM type that were possible and the existence of a cutoff frequency, but no experimental verification was made at the time. The waveguide was then essentially forgotten until it was rediscovered independently in 1936 by two researchers [3]. After preliminary experiments in 1932, George C. Southworth of the AT&T Company in New York presented a paper on the waveguide in 1936. At the same meeting, W. L.

Barrow of MIT presented a paper on the circular waveguide, with experimental confirmation of propagation.

Early RF and microwave systems relied on waveguides, two-wire lines, and coaxial lines for transmission. Waveguides have the advantage of high power-handling capability and low loss but are bulky and expensive, especially at low frequencies. Two-wire lines are inexpensive but lack shielding. Coaxial lines are shielded but are a difficult medium in which to fabricate complex microwave components. Planar transmission lines provide an alternative, in the form of stripline, microstrip lines, slotlines, coplanar waveguides, and several other types of related geometries. Such transmission lines are compact, low in cost, and capable of being easily integrated with active circuit devices, such as diodes and transistors, to form microwave integrated circuits. The first planar transmission line may have been a flat-strip coaxial line, similar to a stripline, used in a production power divider network in World War II [4], but planar lines did not see intensive development until the 1950s. Microstrip lines were developed at ITT laboratories [5] and were competitors of stripline. The first microstrip lines used a relatively thick dielectric substrate, which accentuated the non-TEM mode behavior and frequency dispersion of the line. This characteristic made it less desirable than stripline until the 1960s, when much thinner substrates began to be used. This reduced the frequency dependence of the line, and now microstrip lines are often the preferred medium for microwave integrated circuits.

2. MICROSTRIP LINE

Microstrip line is one of the most popular types of planar transmission lines primarily because it can be fabricated by photolithographic processes and

is easily miniaturized and integrated with both passive and active microwave devices. The geometry of a microstrip line is shown in Figure 3.25a. A conductor of width W is printed on a thin, grounded dielectric substrate of thickness d and relative permittivity ε_r; a sketch of the field lines is shown in Figure 3.25b.

If the dielectric substrate were not present ($\varepsilon_r = 1$), we would have a two-wire line consisting of a flat strip conductor over a ground plane, embedded in a homogeneous medium (air). This would constitute a simple TEM transmission line with phase velocity Up = c and propagation constant $\beta = k0$.

The presence of the dielectric, particularly the fact that the dielectric does not fill the region above the strip ($y > d$), complicates the behavior and analysis of microstrip line. Unlike stripline, where all the fields are contained within a homogeneous dielectric region, microstrip has some (usually most) of its field lines in the dielectric region between the strip conductor and the ground plane and some fraction in the air region above the substrate. For this reason microstrip line cannot support a pure TEM wave since the phase velocity of TEM fields in the dielectric region would be $c/\sqrt{\varepsilon_r}$, while the phase velocity of TEM fields in the air region would be c, so a phase-matching condition at the dielectric–air interface would be impossible to enforce.

In actuality, the exact fields of a microstrip line constitute a hybrid TM-TE wave and require more advanced analysis techniques than we are prepared to deal with here. In most practical applications, however, the dielectric substrate is electrically very thin ($d << \lambda$), and so the fields are quasi-TEM. In other words, the fields are essentially the same as those of the static (DC) case. Thus, good approximations for the phase velocity, propagation constant, and characteristic impedance can be obtained from static, or quasi-static, solutions. Then the phase velocity and propagation constant can be expressed as

$$v_p = \frac{c}{\sqrt{\epsilon_e}}, \tag{3.193}$$

$$\beta = k_0\sqrt{\epsilon_e}, \tag{3.194}$$

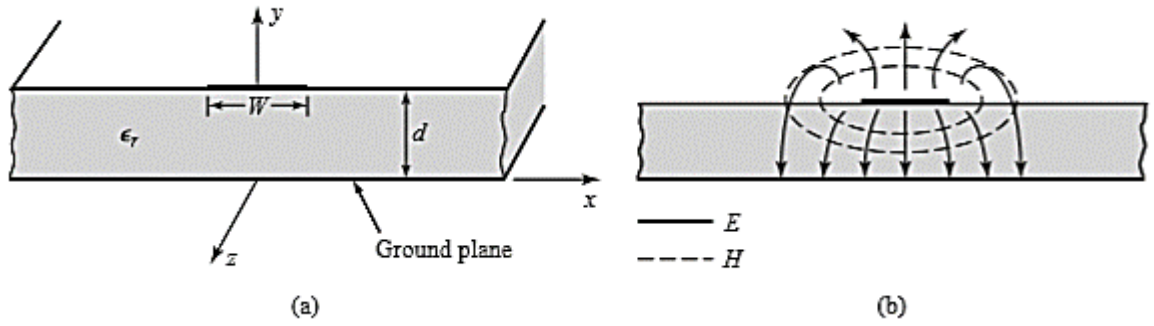

Fig 3.25 - Microstrip transmission line. (a) Geometry. (b) Electric and magnetic field lines.

where ε_e is the effective dielectric constant of the microstrip line. Because some of the field lines are in the dielectric region and some are in air, the effective dielectric constant satisfies the relation

$$1 < \varepsilon_e < \varepsilon_r$$

and depends on the substrate dielectric constant, the substrate thickness, the conductor width, and the frequency.

We will present approximate design formulas for the effective dielectric constant, characteristic impedance, and attenuation of microstrip line; these results are curve-fit approximations to rigorous quasi-static solutions [8, 9]. Then we will discuss additional aspects of microstrip lines, including frequency-dependent effects, higher order modes, and parasitic effects.

2.1. FORMULAS FOR EFFECTIVE DIELECTRIC CONSTANT, CHARACTERISTIC IMPEDANCE, AND ATTENUATION

The effective dielectric constant of a microstrip line is given approximately by

$$\epsilon_e = \frac{\epsilon_r + 1}{2} + \frac{\epsilon_r - 1}{2} \frac{1}{\sqrt{1 + 12d/W}}. \tag{3.195}$$

The effective dielectric constant can be interpreted as the dielectric constant of a homogeneous medium that equivalently replaces the air and dielectric regions of the microstrip line, as shown in Figure 3.26. The phase velocity and propagation constant are then given by (3.193) and (3.194).

Given the dimensions of the microstrip line, the characteristic impedance can be calculated as

$$Z_0 = \begin{cases} \dfrac{60}{\sqrt{\epsilon_e}} \ln\left(\dfrac{8d}{W} + \dfrac{W}{4d}\right) & \text{for } W/d \leq 1 \\ \dfrac{120\pi}{\sqrt{\epsilon_e}\,[W/d + 1.393 + 0.667 \ln(W/d + 1.444)]} & \text{for } W/d \geq 1. \end{cases} \tag{3.196}$$

For a given characteristic impedance Z_0 and dielectric constant ε_r, the W/d ratio can be found as

$$\frac{W}{d} = \begin{cases} \dfrac{8e^A}{e^{2A}-2} & \text{for } W/d < 2 \\ \dfrac{2}{\pi}\left[B - 1 - \ln(2B-1) + \dfrac{\epsilon_r - 1}{2\epsilon_r}\left\{\ln(B-1) + 0.39 - \dfrac{0.61}{\epsilon_r}\right\}\right] & \text{for } W/d > 2, \end{cases} \tag{3.197}$$

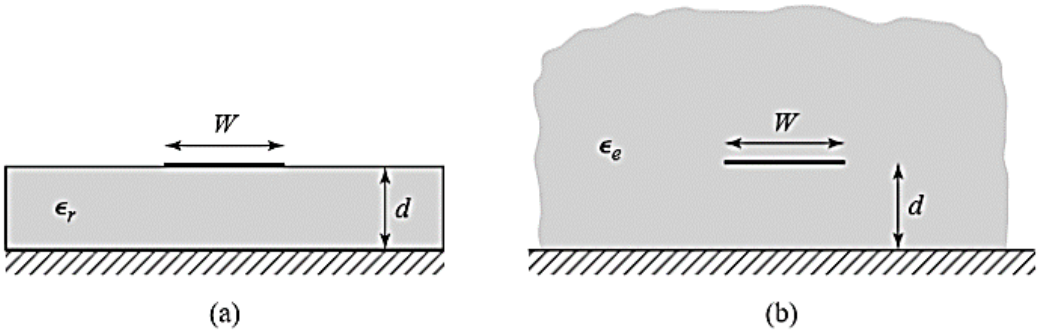

Fig 3.26 - Equivalent geometry of a quasi-TEM microstrip line. (a) Original geometry. (b) Equivalent geometry, where the dielectric substrate of relative permittivity ε_r is replaced with a homogeneous medium of effective relative permittivity ε_e.

Where

$$A = \frac{Z_0}{60}\sqrt{\frac{\epsilon_r + 1}{2}} + \frac{\epsilon_r - 1}{\epsilon_r + 1}\left(0.23 + \frac{0.11}{\epsilon_r}\right)$$

$$B = \frac{377\pi}{2Z_0\sqrt{\epsilon_r}}.$$

Considering a microstrip line as a quasi-TEM line, we can determine the attenuation due to dielectric loss as

$$\alpha_d = \frac{k_0\epsilon_r(\epsilon_e - 1)\tan\delta}{2\sqrt{\epsilon_e}(\epsilon_r - 1)} \text{ Np/m}, \tag{3.198}$$

where tanδ is the loss tangent of the dielectric. This result is derived from (3.30) by multiplying by a “filling factor,”

$$\frac{\epsilon_r(\epsilon_e - 1)}{\epsilon_e(\epsilon_r - 1)},$$

which accounts for the fact that the fields around the microstrip line are partly in air (lossless) and partly in the dielectric (lossy). The attenuation due to conductor loss is given approximately by [8]

$$\alpha_c = \frac{R_s}{Z_0 W} \text{ Np/m}, \qquad (3.199)$$

where Rs =$\sqrt{\omega\mu_0/2\sigma}$ is the surface resistivity of the conductor. For most microstrip substrates, conductor loss is more significant than dielectric loss; exceptions may occur, however, with some semiconductor substrates.

3. REFERENCES

[1] S. Ramo, J. R. Winnery, and T. Van Duzer, Fields and Waves in Communication Electronics, 3rd edition, John Wiley & Sons, New York, 1994.

[2] J. A. Stratton, Electromagnetic Theory, McGraw-Hill, New York, 1941.

[3] H. A. Wheeler, "Reflection Charts Relating to Impedance Matching," IEEE Transactions on Microwave Theory and Techniques, vol. MTT-32, pp. 1008–1021, September 1984.

[4] P. H. Smith, "Transmission Line Calculator," Electronics, vol. 12, No. 1, pp. 29–31, January 1939.

[5] P. J. Nahin,Oliver Heaviside: Sage in Solitude, IEEE Press, New York, 1988.

[6] H. A. Wheeler, "Formulas for the Skin Effect," Proceedings of the IRE, vol. 30, pp. 412–424, September 1942.

[7] T. C. Edwards, Foundations for Microstrip Circuit Design, John Wiley & Sons, New York, 1987.

[8] O. Heaviside, Electromagnetic Theory, Vol. 1, 1893. Reprinted by Dover, New York, 1950.

[9] Lord Rayleigh, "On the Passage of Electric Waves through Tubes," Philosophical Magazine, vol. 43, pp. 125–132, 1897. Reprinted in Collected Papers, Cambridge University Press, Cambridge, 1903.

[10] K. S. Packard, “The Origin of Waveguides: A Case of Multiple Rediscovery,” IEEE Transactions on Microwave Theory and Techniques, vol. MTT-32, pp. 961–969, September 1984.

[11] R. M. Barrett, “Microwave Printed Circuits—An Historical Perspective,” IEEE Transactions on Microwave Theory and Techniques, vol. MTT-32, pp. 983–990, September 1984.

[12] D. D. Grieg and H. F. Englemann, “Microstrip—A New Transmission Technique for the Kilomegacycle Range,” Proceedings of the IRE, vol. 40, pp. 1644–1650, December 1952.

[13] H. Howe, Jr., Stripline Circuit Design, Artech House, Dedham, Mass., 1974.

[14] I. J. Bahl and R. Garg, “A Designer’s Guide to Stripline Circuits,” Microwaves, January 1978, pp. 90–96.

[15] I. J. Bahl and D. K. Trivedi, “A Designer’s Guide to Microstrip Line,” Microwaves, May 1977, pp. 174–182.

[16] K. C. Gupta, R. Garg, and I. J. Bahl, Microstrip Lines and Slotlines, Artech House, Dedham, Mass., 1979.

Chapter 3

1. INTRODUCTION:

In late 1990s the uniplanar EBG structures were developed. Later, these different shapes of EBG structures were reported and a comparison among them was shown. In soft and hard characteristics of EBG structure for TE and TM propagating modes is shown. In a comparison of bandgap characteristics among EBGs and soft surfaces is made. In relationship between EBG and right/left handed structures is shown. 2-D EBG 22 structures have some limits which are discussed in. New configurations of EBG structures are proposed like dumbbell shaped, cylindrical and ellipse shaped and double armed etc. In Low –Temperature Co-fired Ceramic (LTCC) is used for EBG fabrications. In multi-layered EBG structures are discussed. Frequency Selective Surfaces (FSS) were commonly used periodic structures and led to several EBG structure designs. Single band-gap to multi-band-gap EBG structures are proposed in. Due to rapid surge in EBG structure's uses compact EBGs are proposed by researchers in. Different methods used to realize compactness comprised spiral fashioned EBGs, by means of Hilbert curve and complementary proposals. EBG cells that have polarization-dependent reflection phase are conversed in. Tunable EBG structures with varactor diodes and added active components are recommended in. EBG structure optimization procedures like genetic algorithms and particle swarm optimization are defined so as to analyze these structures effortlessly.

2. APPLICATIONS OF EBG STRUCTURES IN EFFICIENT MICROSTRIP ANTENNA DESIGN

Due to certain interesting properties of EBG structures these are now widely used with antenna and microwave circuits to make them efficient. Review papers related to the applications of EBG structures with microwave and antenna circuits can be found in. EBG structures have found enormous applications to minimize the propagation of surface waves in antenna substrates thereby increasing antenna gain and efficiency and reducing back lobes. In the enhancement in antenna bandwidth is reported with the application of EBG structures. These structures also have applications in antenna size reduction and improvement in antenna radiation pattern. EBGs have also been used with antenna arrays primarily to minimize the mutual coupling, which is major cause for reduced antenna efficiency and scan blindness.

2.1. EBG STRUCTURE APPLICATION WITH WIRE AND SLOT ANTENNAS

Next important uses of EBG structures are included in low profile wire antennas. In the band gap of EBG structure due to zero reflection phases the radiation characteristics of antenna near EBG ground plane is significantly improved. Figure 1.7 shows a simple dipole antenna placed above both PEC and EBG ground planes. Figure 1.8 shows the return loss versus frequency plot for both the ground planes. It can be seen that when the PEC is used as a ground plane the magnitude of return loss is around 3.5 dB. The poor value of return loss is due to radiations from dipoles are cancelled by the image current of the ground plane.

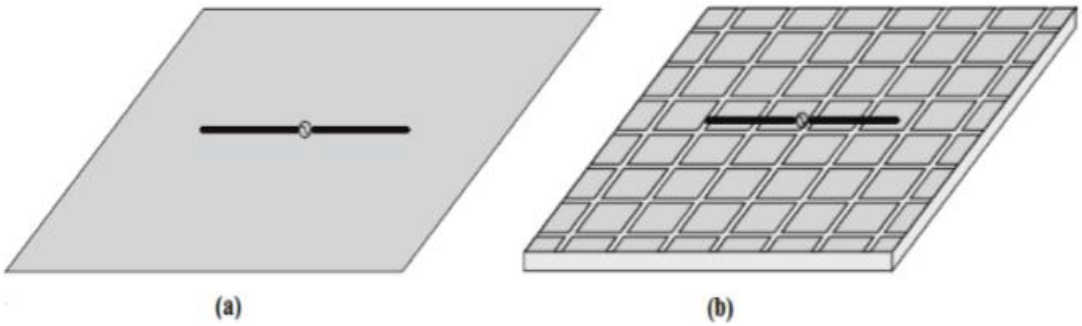

Fig 1.7: A dipole over (a) Conventional Ground, (b) EBGs based ground plane (IEEE 2003).

If PMC surfaces are used as ground plane then there is improvement in the magnitude of return loss and its value now comes around 7.3 dB due to positive value of reflection coefficient from the PMC ground plane. It should also be noted that PMC structures does not occur in nature.

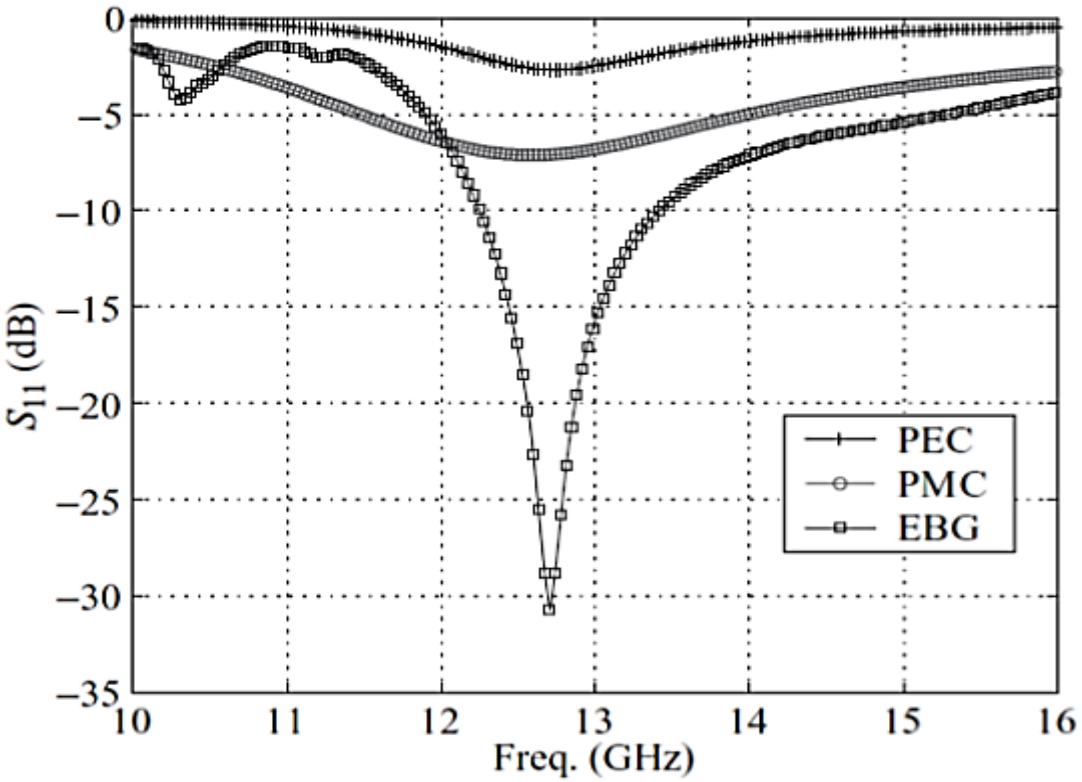

Fig 1.8: Return loss comparisons of PEC, PMC and EBG structures (from IEEE 2003).

The desired value of return loss is obtained when EBG ground planes are used which simultaneously provides positive reflection and minimize surface waves in its band gap. Hence researchers proved that EBG structures have a potentiality to replace PEC as ground plane in low-profile antennas.

In addition EBG structures also find applications with dipole antennas, monopole antennas, spiral shapes antennas, circularly polarized curl antenna, loop antennas, fractal antennas and inverted F type antennas.

Broadband Archimedean spiral antenna with EBG ground plane as a low-profile configuration was reported in. Bow-tie antennas and open sleeve antennas for broadband applications are also discussed with EBG structures in. Mutual coupling reduction in low profile antenna array and curl antenna array is reported in. In slot antennas EBG structures have been used to enhance the radiation characteristics of antennas. A triple band slot antenna with EBG feed is discussed in.

Applications of EBGs with waveguide slot antenna are discussed in.

2.2. EBG STRUCTURE APPLICATION WITH HIGH GAIN ANTENNAS

In applications of EBGs with high gain antenna are discussed. With the applications of EBGs as super states the gain enhancement of antennas are reported in. Circularly polarized antenna with improved antenna bandwidth using EBGs are reported in. Applications of EBGs in design of horn antennas are presented in. In the applications of EBGs in adaptive antennas and beam steering antennas are discussed. Use of EBGs like rectangular shaped, circular shaped and elliptical shaped are used in directive antenna designs and with reflector antenna are reported in.

2.3. EBG STRUCTURE APPLICATION WITH DEVICES USED IN REAL LIFE

Applications of EBGs in base station antennas and mobile handset antennas are shown in. Antennas integrated with EBG structures used with WLAN and microwave links are studied in. EBG antennas for Global Positioning System (GPS) applications are discussed.

EBGs antennas are used with Radio Frequency Identification (RFID) readers, Wearable devices and biotelemetry systems. Furthermore, EBGs has also been used with direction finding applications, radars, Unmanned aerial vehicles (UAV), Waveguides, microwave circuitries and EM interference reductions.

Chapter 4

1. INTRODUCTION:

This chapter marks a turning point, in that we now begin to apply the theory and techniques of previous chapters to practical problems in microwave engineering. We start with the topic of impedance matching, which is often an important part of a larger design process for a microwave component or system. The basic idea of impedance matching is illustrated in Figure 5.1, which shows an impedance matching network placed between a load impedance and a transmission line. The matching network is ideally lossless, to avoid unnecessary loss of power, and is usually designed so that the impedance seen looking into the matching network is Z0. Then reflections will be eliminated on the transmission line to the left of the matching network, although there will usually be multiple reflections between the matching network and the load. This procedure is sometimes referred to as tuning. Impedance matching or tuning is important for the following reasons:

- Maximum power is delivered when the load is matched to the line (assuming the generator is matched), and power loss in the feed line is minimized.
- Impedance matching sensitive receiver components (antenna, low-noise amplifier, etc.) may improve the signal-to-noise ratio of the system.
- Impedance matching in a power distribution network (such as an antenna array feed network) may reduce amplitude and phase errors.

As long as the load impedance, ZL, has a positive real part, a matching network can always be found. Many choices are available, however, and we will discuss the design and performance of several types of practical matching networks. Factors that may be important in the selection of a particular matching network include the following:

- *Complexity*—As with most engineering solutions, the simplest design that satisfies the required specifications is generally preferable. A simpler matching network is usually cheaper, smaller, more reliable, and less lossy than a more complex design.
- *Bandwidth*—Any type of matching network can ideally give a perfect match (zero reflection) at a single frequency. In many applications, however, it is desirable to match a load over a band of frequencies. There are several ways of doing this, with, of course, a corresponding increase in complexity.
- *Implementation*—Depending on the type of transmission line or waveguide being used, one type of matching network may be preferable to another. For example, tuning stubs are much easier to implement in waveguide than are multisection quarter-wave transformers.
- *Adjustability*—In some applications the matching network may require adjustment to match a variable load impedance. Some types of matching networks are more amenable than others in this regard.

Fig 5.1 - A lossless network matching an arbitrary load impedance to a transmission line.

2. THE QUARTER WAVE TRANSFORMER

The quarter wave transformer is a useful and practical circuit for Impedance Matching and also provides a simple transmission line circuit that father illustrate the properties of standing waves on a mismatched line. Although we will study the design and performance of quarter wave matching Transformers more extensively in chapter 5 the main purpose here is the application of the previously developed transmission line theory to a basic transmission line circuit. we will first approach the problem from the impedance viewpoint, and then so how this result can also be interpreted in terms of an infinite set of multiple reflections on the matching section.

2.1. THE IMPEDANCE VIEWPOINT

Figure 2.16 shows a circuit employing a quarter-wave transformer. The load resistance R_L and the feedline characteristic impedance Z_0 are both real and assumed to be known. These two components are connected with a lossless piece of transmission line of (unknown) characteristic impedance Z_1

and length λ/4. It is desired to match the load to the Z_0 line by using the λ/4 section of line and so make Γ =0 looking into the λ/4 matching section. From (2.44) the input impedance Zin can be found as

$$Z_{\text{in}} = Z_1 \frac{R_L + jZ_1 \tan \beta\ell}{Z_1 + jR_L \tan \beta\ell}. \tag{2.61}$$

To evaluate this for $\beta\ell = (2\pi/\lambda)\,(\lambda/4) = \pi/2$, we can divide the numerator and denominator by $\tan\beta\ell$ and take the limit as $\beta\ell \to \pi/2$ to get

$$Z_{\text{in}} = \frac{Z_1^2}{R_L}. \tag{2.62}$$

In order for Γ = 0, we must have $Z_{in} = Z_0$, which yields the characteristic impedance Z_1 as

$$Z_1 = \sqrt{Z_0 R_L}, \tag{2.63}$$

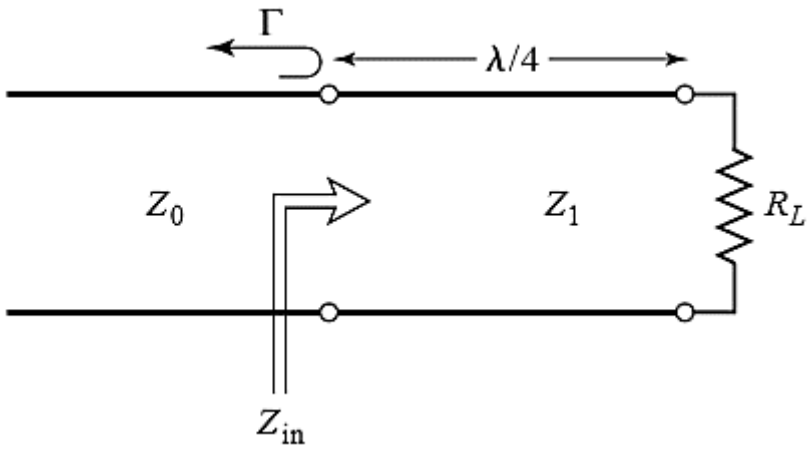

Fig 2.16 - The quarter-wave matching transformer

which is the geometric mean of the load and source impedances. Then there will be no standing waves on the feedline (SWR = 1), although there will be standing waves on the λ/4 matching section. In addition, the above condition applies only when the length of the matching section is λ/4 or an odd multiple of λ/4, long, so that a perfect match may be achieved at one frequency, but impedance mismatch will occur at other frequencies.

2.2. THE MULTIPLE-REFLECTION VIEWPOINT

Figure 2.18 shows the quarter-wave transformer circuit with reflection and transmission coefficients defined as follows:

Γ =overall, or total, reflection coefficient of a wave incident on the λ/4 transformer (same as Γ in Example 2.5).

Γ1 =partial reflection coefficient of a wave incident on a load Z_1, from the Z_0 line.

Γ2 =partial reflection coefficient of a wave incident on a load Z_0, from theZ_1 line.

Γ3 =partial reflection coefficient of a wave incident on a load R_L, from the Z_1 line.

T1 =partial transmission coefficient of a wave from the Z_0 line into the Z_1 line.

T2 =partial transmission coefficient of a wave from the Z_1 line into the Z_0 line.

These coefficients can be expressed as

$$\Gamma_1 = \frac{Z_1 - Z_0}{Z_1 + Z_0}, \tag{2.64a}$$

$$\Gamma_2 = \frac{Z_0 - Z_1}{Z_0 + Z_1} = -\Gamma_1, \tag{2.64b}$$

$$\Gamma_3 = \frac{R_L - Z_1}{R_L + Z_1}, \tag{2.64c}$$

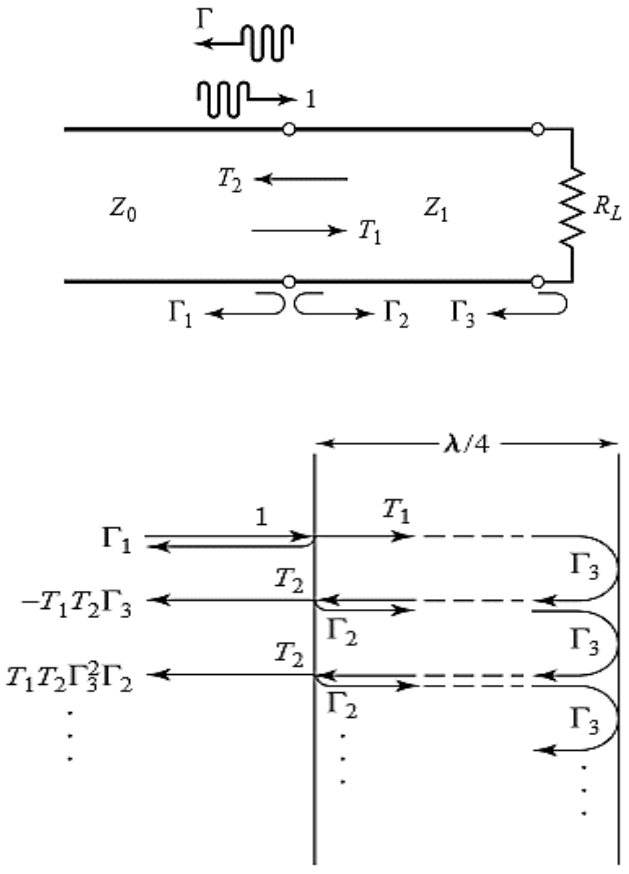

Fig 2.18 - Multiple reflection analysis of the quarter-wave transformer.

$$T_1 = \frac{2Z_1}{Z_1 + Z_0}, \tag{2.64d}$$

$$T_2 = \frac{2Z_0}{Z_1 + Z_0}. \tag{2.64e}$$

Now think of the quarter-wave transformer of Figure 2.18 in the time domain, and imagine a wave traveling down the Z_0 feedline toward the transformer. When the wave first hits the junction with the Z_1 line, it sees only an impedance Z_1 since it has not yet traveled to the load R_L and cannot see that effect. Part of the wave is reflected with a coefficient Γ_1, and part is transmitted onto the Z_1 line with a coefficient T_1. The transmitted wave then travels $\lambda/4$ to the load, is reflected with a coefficient Γ_3, and travels another $\lambda/4$ back to the junction with the Z_0 line. Part of this wave is transmitted through (to the left) to the Z_0 line, with coefficient T_2, and part is reflected back toward the load with coefficient Γ_2. Clearly, this process continues with an infinite number of bouncing waves, and the total reflection coefficient, Γ, is the sum of all of these partial reflections. Since each round-trip path up and down the $\lambda/4$ transformer section results in a 180° phase shift, the total reflection coefficient can be expressed as

$$\begin{aligned}\Gamma &= \Gamma_1 - T_1T_2\Gamma_3 + T_1T_2\Gamma_2\Gamma_3^2 - T_1T_2\Gamma_2^2\Gamma_3^3 + \cdots \\ &= \Gamma_1 - T_1T_2\Gamma_3 \sum_{n=0}^{\infty} (-\Gamma_2\Gamma_3)^n. \end{aligned} \tag{2.65}$$

Since $|\Gamma_3| < 1$ and $|\Gamma_2| < 1$, the infinite series in (2.65) can be summed using the geometric series result that

$$\sum_{n=0}^{\infty} x^n = \frac{1}{1-x}, \qquad \text{for } |x| < 1,$$

to give

$$\Gamma = \Gamma_1 - \frac{T_1 T_2 \Gamma_3}{1 + \Gamma_2 \Gamma_3} = \frac{\Gamma_1 + \Gamma_1 \Gamma_2 \Gamma_3 - T_1 T_2 \Gamma_3}{1 + \Gamma_2 \Gamma_3}. \tag{2.66}$$

The numerator of this expression can be simplified using (2.64) to give

$$\begin{aligned}
\Gamma_1 - \Gamma_3(\Gamma_1^2 + T_1 T_2) &= \Gamma_1 - \Gamma_3\left[\frac{(Z_1 - Z_0)^2}{(Z_1 + Z_0)^2} + \frac{4Z_1 Z_0}{(Z_1 + Z_0)^2}\right] \\
&= \Gamma_1 - \Gamma_3 = \frac{(Z_1 - Z_0)(R_L + Z_1) - (R_L - Z_1)(Z_1 + Z_0)}{(Z_1 + Z_0)(R_L + Z_1)} \\
&= \frac{2(Z_1^2 - Z_0 R_L)}{(Z_1 + Z_0)(R_L + Z_1)},
\end{aligned}$$

which is seen to vanish if we choose $Z1 = \sqrt{(Z_0)}\ (R_L)$, as in (2.63). Then Γ of (2.66) is zero, and the line is matched. This analysis shows that the matching property of the quarter-wave transformer comes about by properly selecting the

characteristic impedance and length of the matching section so that the superposition of all of the partial reflections adds to zero. Under steady-state conditions, an infinite sum of waves traveling in the same direction with the same phase velocity can be combined into a single traveling wave. Thus, the infinite set of waves traveling in the forward and reverse directions on the matching section can be reduced to two waves traveling in opposite directions. See Problem 2.25.

As introduced in Section 2.5, the quarter-wave transformer is a simple and useful circuit for matching a real load impedance to a transmission line. An additional feature of the quarter-wave transformer is that it can be extended to multisection designs in a methodical manner to provide broader bandwidth. If only a narrow band impedance match is required, a single-section transformer may suffice. However, as we will see in the next few sections, multisection quarter-wave transformer designs can be synthesized to yield optimum matching characteristics over a desired frequency band. We will see in Chapter 8 that such networks are closely related to bandpass filters.

One drawback of the quarter-wave transformer is that it can only match a real load impedance. A complex load impedance can always be transformed into a real impedance, however, by using an appropriate length of transmission line between the load and the transformer, or an appropriate series or shunt reactive element. These techniques will usually alter the frequency dependence of the load, and this often has the effect of reducing the bandwidth of the match.

In Section 2.5 we analyzed the operation of a quarter-wave transformer from both an impedance viewpoint and a multiple reflection viewpoint. Here we will concentrate on the bandwidth performance of the transformer as a function of the load mismatch; this

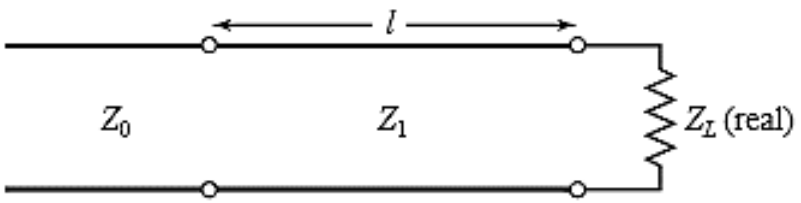

Fig 5.10 - A single-section quarter-wave matching transformer. $\ell = \lambda_0/4$ at the design frequency f_0.

discussion will also serve as a prelude to the more general case of multisection transformers in the sections to follow.

The single-section quarter-wave matching transformer circuit is shown in Figure 5.10, with the characteristic impedance of the matching section given as

$$Z_1 = \sqrt{Z_0 Z_L}. \tag{5.25}$$

At the design frequency, f_0, the electrical length of the matching section is $\lambda_0/4$, but at other frequencies the length is different, so a perfect match is no longer obtained. We will derive an approximate expression for the resulting impedance mismatch versus frequency.

The input impedance seen looking into the matching section is

$$Z_{\text{in}} = Z_1 \frac{Z_L + jZ_1 t}{Z_1 + jZ_L t}, \tag{5.26}$$

where $t = \tan\beta\ell = \tan\theta$, and $\beta\ell = \theta = \pi/2$ at the design frequency f_0. The resulting reflection coefficient is

$$\Gamma = \frac{Z_{\text{in}} - Z_0}{Z_{\text{in}} + Z_0} = \frac{Z_1(Z_L - Z_0) + jt\left(Z_1^2 - Z_0 Z_L\right)}{Z_1(Z_L + Z_0) + jt\left(Z_1^2 + Z_0 Z_L\right)}. \tag{5.27}$$

Because $Z^2_1 = Z_0 Z_L$, this reduces to

$$\Gamma = \frac{Z_L - Z_0}{Z_L + Z_0 + j2t\sqrt{Z_0 Z_L}}. \tag{5.28}$$

The reflection coefficient magnitude is

$$\begin{aligned} |\Gamma| &= \frac{|Z_L - Z_0|}{\left[(Z_L + Z_0)^2 + 4t^2 Z_0 Z_L\right]^{1/2}} \\ &= \frac{1}{\left\{(Z_L + Z_0)^2/(Z_L - Z_0)^2 + [4t^2 Z_0 Z_L/(Z_L - Z_0)^2]\right\}^{1/2}} \\ &= \frac{1}{\left\{1 + [4Z_0 Z_L/(Z_L - Z_0)^2] + [4Z_0 Z_L t^2/(Z_L - Z_0)^2]\right\}^{1/2}} \\ &= \frac{1}{\left\{1 + [4Z_0 Z_L/(Z_L - Z_0)^2]\ \sec^2\theta\right\}^{1/2}}, \end{aligned} \tag{5.29}$$

since $1+t^2 = 1+\tan^2\theta = \sec^2\theta$.

If we assume that the operating frequency is near the design frequency f_0, then $\ell \approx \lambda_0/4$ and $\theta \approx \pi/2$. Then $\sec^2\theta >> 1$, and (5.29) simplifies to

$$|\Gamma| \simeq \frac{|Z_L - Z_0|}{2\sqrt{Z_0 Z_L}} |\cos\theta| \quad \text{for } \theta \text{ near } \pi/2. \tag{5.30}$$

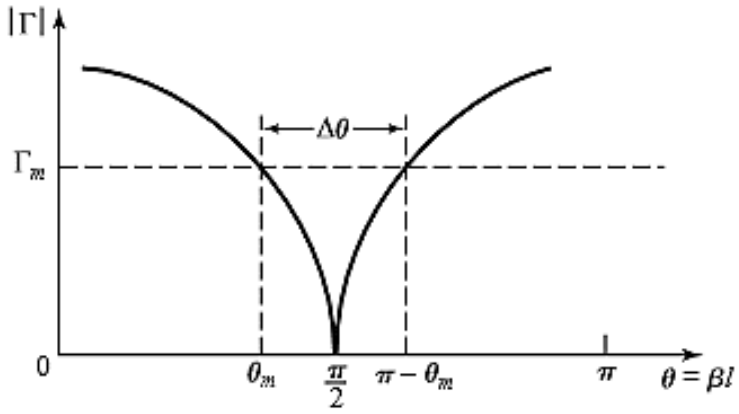

Fig 5.11 - Approximate behavior of the reflection coefficient magnitude for a single-section quarter-wave transformer operating near its design frequency.

This result gives the approximate mismatch of the quarter-wave transformer near the design frequency, as sketched in Figure 5.11.

If we set a maximum value, Γ_m, for an acceptable reflection coefficient magnitude, then the bandwidth of the matching transformer can be defined as

$$\Delta\theta = 2\left(\frac{\pi}{2} - \theta_m\right), \tag{5.31}$$

since the response of (5.29) is symmetric about $\theta = \pi/2$, and $\Gamma = \Gamma_m$ at $\theta = \theta_m$ and at $\theta = \pi - \theta_m$. Equating Γ_m to the exact expression for the reflection coefficient magnitude in (5.29) allows us to solve for θ_m:

$$\frac{1}{\Gamma_m^2} = 1 + \left(\frac{2\sqrt{Z_0 Z_L}}{Z_L - Z_0}\sec\theta_m\right)^2,$$

Or

$$\cos\theta_m = \frac{\Gamma_m}{\sqrt{1-\Gamma_m^2}} \frac{2\sqrt{Z_0 Z_L}}{|Z_L - Z_0|}. \tag{5.32}$$

If we assume TEM lines, then

$$\theta = \beta\ell = \frac{2\pi f}{v_p} \frac{v_p}{4f_0} = \frac{\pi f}{2f_0},$$

and so the frequency of the lower band edge at $\theta = \theta_m$ is

$$f_m = \frac{2\theta_m f_0}{\pi},$$

and the fractional bandwidth is, using (5.32),

$$\begin{aligned} \frac{\Delta f}{f_0} &= \frac{2(f_0 - f_m)}{f_0} = 2 - \frac{2f_m}{f_0} = 2 - \frac{4\theta_m}{\pi} \\ &= 2 - \frac{4}{\pi}\cos^{-1}\left[\frac{\Gamma_m}{\sqrt{1-\Gamma_m^2}} \frac{2\sqrt{Z_0 Z_L}}{|Z_L - Z_0|}\right]. \end{aligned} \tag{5.33}$$

Fractional bandwidth is usually expressed as a percentage, $100\Delta f/f_0\%$. Note that the bandwidth of the transformer increases as Z_L becomes closer to Z_0 (a less mismatched load).

The above results are strictly valid only for TEM lines. When non-TEM lines (such as waveguides) are used, the propagation constant is no longer a linear function of frequency, and the wave impedance will be frequency dependent. These factors serve to complicate the general behavior of quarter-wave transformers for non-TEM lines, but in practice the bandwidth of the transformer is often small enough that these complications do not substantially affect the result. Another factor ignored in the above analysis is the effect of reactances associated with discontinuities when there is a step change in the dimensions of a transmission line. This can often be compensated by making a small adjustment in the length of the matching section.

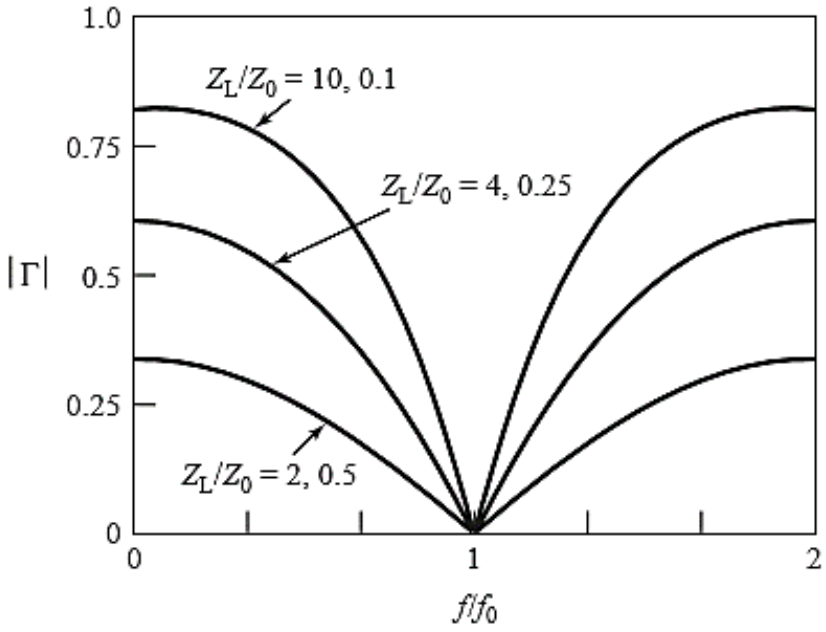

Fig 5.12 - Reflection coefficient magnitude versus frequency for a single-section quarter-wave matching transformer with various load mismatches.

Figure 5.12 shows a plot of the reflection coefficient magnitude versus normalized frequency for various mismatched loads. Note the trend of increased bandwidth for smaller load mismatches.

3. THE THEORY OF SMALL REFLECTION

The quarter-wave transformer provides a simple means of matching any real load impedance to any transmission line impedance. For applications requiring more bandwidth than a single quarter-wave section can provide, multisection transformers can be used. The design of such transformers is the subject of the next two sections, but prior to that material we need to derive some approximate results for the total reflection coefficient caused by the partial reflections from several small discontinuities. This topic is generally referred to as the theory of small reflections [1].

3.1. SINGLE-SECTION TRANSFORMER

We will derive an approximate expression for the overall reflection coefficient, Γ, for the single-section matching transformer shown in Figure 5.13. The partial reflection and transmission coefficients are

$$\Gamma_1 = \frac{Z_2 - Z_1}{Z_2 + Z_1}, \tag{5.34}$$

$$\Gamma_2 = -\Gamma_1, \tag{5.35}$$

$$\Gamma_3 = \frac{Z_L - Z_2}{Z_L + Z_2}, \tag{5.36}$$

$$T_{21} = 1 + \Gamma_1 = \frac{2Z_2}{Z_1 + Z_2}, \tag{5.37}$$

$$T_{12} = 1 + \Gamma_2 = \frac{2Z_1}{Z_1 + Z_2}. \tag{5.38}$$

We can compute the total reflection, Γ, seen by the feed line using either the impedance method, or the multiple reflection method, as discussed in Section 2.5. For our present

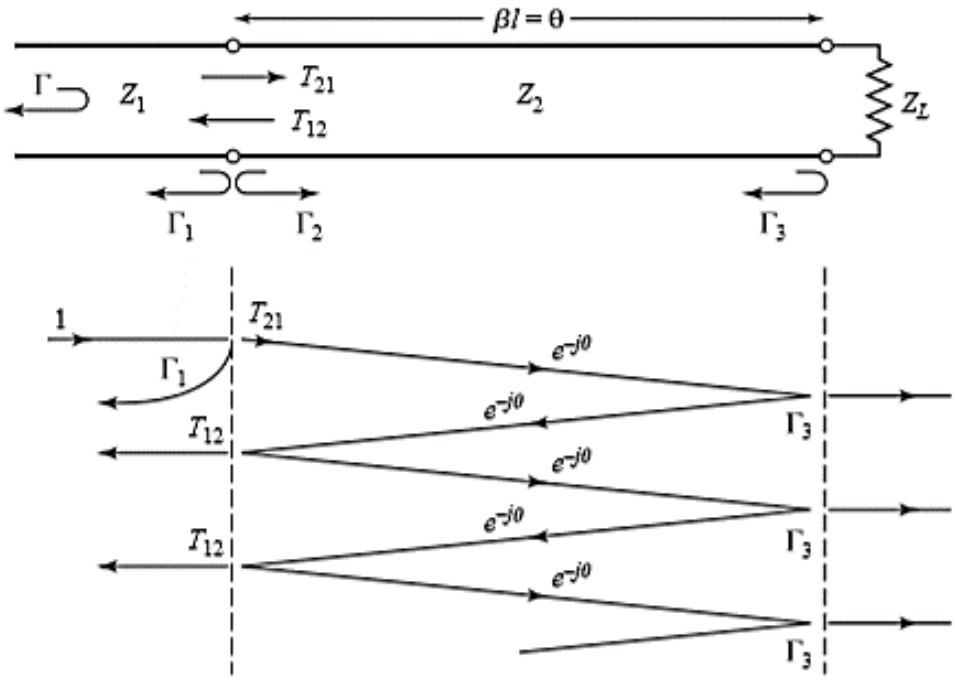

Fig 5.13 - Partial reflections and transmissions on a single-section matching transformer.

purpose the latter technique is preferred, so we express the total reflection as an infinite sum of partial reflections and transmissions as follows:

$$\begin{aligned}\Gamma &= \Gamma_1 + T_{12}T_{21}\Gamma_3 e^{-2j\theta} + T_{12}T_{21}\Gamma_3^2\Gamma_2 e^{-4j\theta} + \cdots \\ &= \Gamma_1 + T_{12}T_{21}\Gamma_3 e^{-2j\theta}\sum_{n=0}^{\infty}\Gamma_2^n\Gamma_3^n e^{-2jn\theta}. \end{aligned} \tag{5.39}$$

The summation of the geometric series

$$\sum_{n=0}^{\infty} x^n = \frac{1}{1-x} \quad \text{for } |x| < 1$$

allows us to express (5.39) in closed form as

$$\Gamma = \Gamma_1 + \frac{T_{12}T_{21}\Gamma_3 e^{-2j\theta}}{1 - \Gamma_2\Gamma_3 e^{-2j\theta}}. \tag{5.40}$$

From (5.35), (5.37), and (5.38), we use $\Gamma_2 = -\Gamma_1$, $T_{21} = 1+\Gamma_1$, and $T_{12} = 1-\Gamma_1$ in (5.40) to give

$$\Gamma = \frac{\Gamma_1 + \Gamma_3 e^{-2j\theta}}{1 + \Gamma_1\Gamma_3 e^{-2j\theta}}. \tag{5.41}$$

If the discontinuities between the impedances Z_1, Z_2 and Z_2, Z_L are small, then $|\Gamma_1\Gamma_3|=1$, so we can approximate (5.41) as

$$\Gamma \simeq \Gamma_1 + \Gamma_3 e^{-2j\theta}. \tag{5.42}$$

This result expresses the intuitive idea that the total reflection is dominated by the reflection from the initial discontinuity between Z_1 and Z_2 (Γ_1), and the first reflection from the discontinuity between Z_2 and Z_L ($\Gamma_3 e^{-2j\theta}$). The $e^{-2j\theta}$ term accounts for the phase delay when the incident wave travels up and down the line. The accuracy of this approximation is illustrated in Problem 5.14.

3.2. MULTISECTION TRANSFORMER

Now consider the multisection transformer shown in Figure 5.14, which consists of N equal-length (commensurate) sections of transmission lines. We will derive an approximate expression for the total reflection coefficient Γ.

Partial reflection coefficients can be defined at each junction, as follows:

$$\Gamma_0 = \frac{Z_1 - Z_0}{Z_1 + Z_0}, \tag{5.43a}$$

$$\Gamma_n = \frac{Z_{n+1} - Z_n}{Z_{n+1} + Z_n}, \tag{5.43b}$$

$$\Gamma_N = \frac{Z_L - Z_N}{Z_L + Z_N}. \tag{5.43c}$$

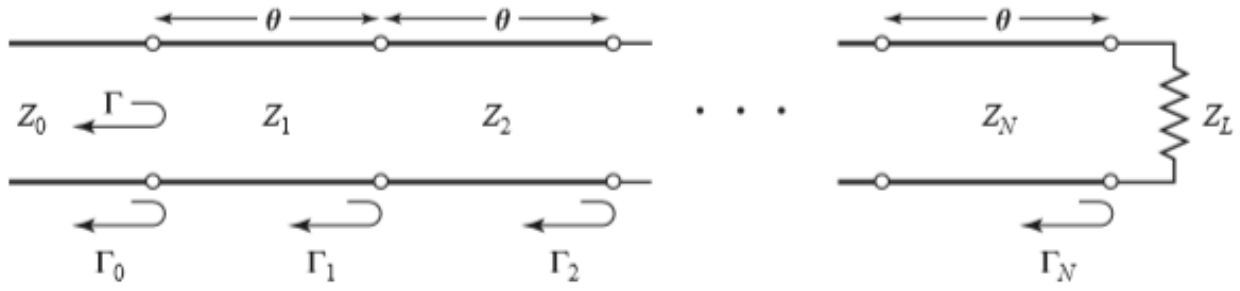

Fig 5.14 - Partial reflection coefficients for a multisection matching transformer.

We also assume that all Z_n increase or decrease monotonically across the transformer and that Z_L is real. This implies that all Γ_n will be real and of the same sign ($\Gamma_n > 0$ if $Z_L > Z_0$; $\Gamma_n < 0$ if $Z_L < Z_0$). Using the results of the previous section allows us to approximate the overall reflection coefficient as

$$\Gamma(\theta) = \Gamma_0 + \Gamma_1 e^{-2j\theta} + \Gamma_2 e^{-4j\theta} + \cdots + \Gamma_N e^{-2jN\theta}. \tag{5.44}$$

Further assume that the transformer can be made symmetrical, so that $\Gamma_0 = \Gamma_N$, $\Gamma_1 = \Gamma_{N-1}$, $\Gamma_2 = \Gamma_{N-2}$, and so on. (Note that this does not imply that the Z_n are symmetrical.) Then (5.44) can be written as

$$\Gamma(\theta) = e^{-jN\theta}\left\{\Gamma_0[e^{jN\theta} + e^{-jN\theta}] + \Gamma_1[e^{j(N-2)\theta} + e^{-j(N-2)\theta}] + \cdots\right\}. \qquad (5.45)$$

If N is odd, the last term is $\Gamma_{(N-1)}/2^{(ej\theta + e-j\theta)}$, while if N is even, the last term is $\Gamma_{N/2}$. Equation (5.45) is seen to be of the form of a finite Fourier cosine series in θ, which can be written as

$$\Gamma(\theta) = 2e^{-jN\theta}\left[\Gamma_0 \cos N\theta + \Gamma_1 \cos(N-2)\theta + \cdots + \Gamma_n \cos(N-2n)\theta + \cdots + \frac{1}{2}\Gamma_{N/2}\right] \quad \text{for } N \text{ even}, \qquad (5.46a)$$

$$\Gamma(\theta) = 2e^{-jN\theta}[\Gamma_0 \cos N\theta + \Gamma_1 \cos(N-2)\theta + \cdots + \Gamma_n \cos(N-2n)\theta + \cdots + \Gamma_{(N-1)/2} \cos\theta] \quad \text{for } N \text{ odd}. \qquad (5.46b)$$

The importance of these results lies in the fact that we can synthesize any desired reflection coefficient response as a function of frequency (θ) by properly choosing the n and using enough sections (N). This should be clear from the realization that a Fourier series can approximate an arbitrary smooth function if enough terms are used. In the next two sections we will show how to use this theory to design multisection transformers for two of the most commonly used passband responses: the binomial (maximally flat) response, and the Chebyshev (equal-ripple) response.

4. BINOMIAL MULTISECTION MATCHING TRANSFORMERS

The passband response (the frequency band where a good impedance match is achieved) of a binomial matching transformer is optimum in the sense that, for a given number of sections, the response is as flat as possible near the design frequency. This type of response, which is also known as maximally flat, is determined for an N-section transformer by setting the first N −1 derivatives of $|\Gamma(\theta)|$ to zero at the center frequency, f_0. Such a response can be obtained with a reflection coefficient of the following form:

$$\Gamma(\theta) = A(1 + e^{-2j\theta})^N. \tag{5.47}$$

Then the reflection coefficient magnitude is

$$\begin{aligned} |\Gamma(\theta)| &= |A||e^{-j\theta}|^N |e^{j\theta} + e^{-j\theta}|^N \\ &= 2^N |A||\cos\theta|^N \end{aligned} \tag{5.48}$$

Note that $|\Gamma(\theta)|=0$ for $\theta = \pi/2$, and that $d^n |\Gamma(\theta)|/d\theta^n = 0$ at $\theta = \pi/2$ for n = 1, 2..., N −1. ($\theta = \pi/2$ corresponds to the center frequency, f_0, for which $\ell = \lambda/4$ and $\theta = \beta\ell = \pi/2$.)

We can determine the constant A by letting $f \rightarrow 0$. Then $\theta = \beta\ell = 0$, and (5.47) reduces to

$$\Gamma(0) = 2^N A = \frac{Z_L - Z_0}{Z_L + Z_0},$$

since for f = 0 all sections are of zero electrical length. The constant A can then be written as

$$A = 2^{-N}\frac{Z_L - Z_0}{Z_L + Z_0}. \tag{5.49}$$

Next we expand Γ(θ) in (5.47) according to the binomial expansion:

$$\Gamma(\theta) = A(1 + e^{-2j\theta})^N = A\sum_{n=0}^{N} C_n^N e^{-2jn\theta}, \tag{5.50}$$

Where

$$C_n^N = \frac{N!}{(N-n)!n!} \tag{5.51}$$

are the binomial coefficients. Note that $C^N_n = C^N_{N-n}$, $C^N_0 = 1$, and $C^N_1 = N = C^N_{N-1}$. The key step is now to equate the desired passband response, given by (5.50), to the actual response as given (approximately) by (5.44):

$$\Gamma(\theta) = A\sum_{n=0}^{N} C_n^N e^{-2jn0} = \Gamma_0 + \Gamma_1 e^{-2j0} + \Gamma_2 e^{-4j0} + \cdots + \Gamma_N e^{-2jN0}.$$

This shows that the n must be chosen as

$$\Gamma_n = AC_n^N. \tag{5.52}$$

where A is given by (5.49) and C^N_n is a binomial coefficient.

At this point, the characteristic impedances, Z_n, can be found via (5.43), but a simpler solution can be obtained using the following approximation [1]. Because we assumed that the Γ_n are small, we can write

$$\Gamma_n = \frac{Z_{n+1} - Z_n}{Z_{n+1} + Z_n} \simeq \frac{1}{2} \ln \frac{Z_{n+1}}{Z_n},$$

since $\ln x \approx 2(x-1)/(x+1)$ for x close to unity. Then, using (5.52) and (5.49) gives

$$\ln \frac{Z_{n+1}}{Z_n} \simeq 2\Gamma_n = 2AC_n^N = 2(2^{-N})\frac{Z_L - Z_0}{Z_L + Z_0} C_n^N \simeq 2^{-N} C_n^N \ln \frac{Z_L}{Z_0}, \qquad (5.53)$$

which can be used to find Z_{n+1}, starting with n = 0. This technique has the advantage of ensuring self-consistency, in that Z_{N+1} computed from (5.53) will be equal to Z_L, as it should. Exact design results, including the effect of multiple reflections in each section, can be found by using the transmission line equations for each section and numerically solving for the characteristic impedances [2]. The results of such calculations are listed in Table 5.1, which gives the exact line impedances for N = 2-, 3-, 4-, 5-, and 6-section binomial matching transformers for various ratios of load impedance, Z_L, to feed line impedance, Z_0. The table gives results only for $Z_L/Z_0 > 1$; if $Z_L/Z_0 < 1$, the results for Z_0/Z_L should be used but with Z_1 starting at the load end. This is because the solution is symmetric about $Z_L/Z_0 = 1$; the same transformer that matches Z_L to Z_0 can be reversed and used to match Z_0 to Z_L. More extensive tables can be found in reference [2].

The bandwidth of the binomial transformer can be evaluated as follows. As in Section 5.4, let m be the maximum value of reflection coefficient that can be tolerated over the passband. Then from (5.48),

$$\Gamma_m = 2^N |A| \cos^N \theta_m,$$

where $\theta_m < \pi/2$ is the lower edge of the passband, as shown in Figure 5.11. Thus,

$$\theta_m = \cos^{-1}\left[\frac{1}{2}\left(\frac{\Gamma_m}{|A|}\right)^{1/N}\right], \tag{5.54}$$

and using (5.33) gives the fractional bandwidth as

$$\begin{aligned}\frac{\Delta f}{f_0} &= \frac{2(f_0 - f_m)}{f_0} = 2 - \frac{4\theta_m}{\pi} \\ &= 2 - \frac{4}{\pi}\cos^{-1}\left[\frac{1}{2}\left(\frac{\Gamma_m}{|A|}\right)^{1/N}\right].\end{aligned} \tag{5.55}$$

TABLE 5.1 Binomial Transformer Design

	$N=2$		$N=3$			$N=4$			
Z_L/Z_0	Z_1/Z_0	Z_2/Z_0	Z_1/Z_0	Z_2/Z_0	Z_3/Z_0	Z_1/Z_0	Z_2/Z_0	Z_3/Z_0	Z_4/Z_0
1.0	1.0000	1.0000	1.0000	1.0000	1.0000	1.0000	1.0000	1.0000	1.0000
1.5	1.1067	1.3554	1.0520	1.2247	1.4259	1.0257	1.1351	1.3215	1.4624
2.0	1.1892	1.6818	1.0907	1.4142	1.8337	1.0444	1.2421	1.6102	1.9150
3.0	1.3161	2.2795	1.1479	1.7321	2.6135	1.0718	1.4105	2.1269	2.7990
4.0	1.4142	2.8285	1.1907	2.0000	3.3594	1.0919	1.5442	2.5903	3.6633
6.0	1.5651	3.8336	1.2544	2.4495	4.7832	1.1215	1.7553	3.4182	5.3500
8.0	1.6818	4.7568	1.3022	2.8284	6.1434	1.1436	1.9232	4.1597	6.9955
10.0	1.7783	5.6233	1.3409	3.1623	7.4577	1.1613	2.0651	4.8424	8.6110

	$N=5$					$N=6$					
Z_L/Z_0	Z_1/Z_0	Z_2/Z_0	Z_3/Z_0	Z_4/Z_0	Z_5/Z_0	Z_1/Z_0	Z_2/Z_0	Z_3/Z_0	Z_4/Z_0	Z_5/Z_0	Z_6/Z_0
1.0	1.0000	1.0000	1.0000	1.0000	1.0000	1.0000	1.0000	1.0000	1.0000	1.0000	1.0000
1.5	1.0128	1.0790	1.2247	1.3902	1.4810	1.0064	1.0454	1.1496	1.3048	1.4349	1.4905
2.0	1.0220	1.1391	1.4142	1.7558	1.9569	1.0110	1.0790	1.2693	1.5757	1.8536	1.9782
3.0	1.0354	1.2300	1.7321	2.4390	2.8974	1.0176	1.1288	1.4599	2.0549	2.6577	2.9481
4.0	1.0452	1.2995	2.0000	3.0781	3.8270	1.0225	1.1661	1.6129	2.4800	3.4302	3.9120
6.0	1.0596	1.4055	2.4495	4.2689	5.6625	1.0296	1.2219	1.8573	3.2305	4.9104	5.8275
8.0	1.0703	1.4870	2.8284	5.3800	7.4745	1.0349	1.2640	2.0539	3.8950	6.3291	7.7302
10.0	1.0789	1.5541	3.1623	6.4346	9.2687	1.0392	1.2982	2.2215	4.5015	7.7030	9.6228

5. CHEBYSHEV MULTISECTION MATCHING TRANSFORMERS

In contrast with the binomial transformer, the multisection Chebyshev matching transformer optimizes bandwidth at the expense of passband ripple. Compromising on the flatness of the passband response leads to a bandwidth that is substantially better than that of the binomial transformer for a given number of sections. The Chebyshev transformer is designed by equating $\Gamma(\theta)$ to a Chebyshev polynomial, which has the optimum characteristics needed for this type of transformer. We will first discuss the properties of Chebyshev

polynomials and then derive a design procedure for Chebyshev matching transformers using the small-reflection theory of Section 5.5.

5.1. CHEBYSHEV POLYNOMIALS

The nth-order Chebyshev polynomial is a polynomial of degree n, denoted by $T_n(x)$. The first four Chebyshev polynomials are

$$T_1(x) = x, \tag{5.56a}$$
$$T_2(x) = 2x^2 - 1, \tag{5.56b}$$
$$T_3(x) = 4x^3 - 3x, \tag{5.56c}$$
$$T_4(x) = 8x^4 - 8x^2 + 1. \tag{5.56d}$$

Higher order polynomials can be found using the following recurrence formula:

$$T_n(x) = 2x\,T_{n-1}(x) - T_{n-2}(x). \tag{5.57}$$

The first four Chebyshev polynomials are plotted in Figure 5.16, from which the following very useful properties of Chebyshev polynomials can be noted:

- For $-1 \leq x \leq 1$, $|T_n(x)| \leq 1$. In this range the Chebyshev polynomials oscillate between ±1. This is the equal-ripple property, and this region will be mapped to the passband of the matching transformer.

- For |x| >1, $|T_n(x)|$ >1. This region will map to the frequency range outside the passband.
- For |x| >1, the $|T_n(x)|$increases faster with x as n increases.

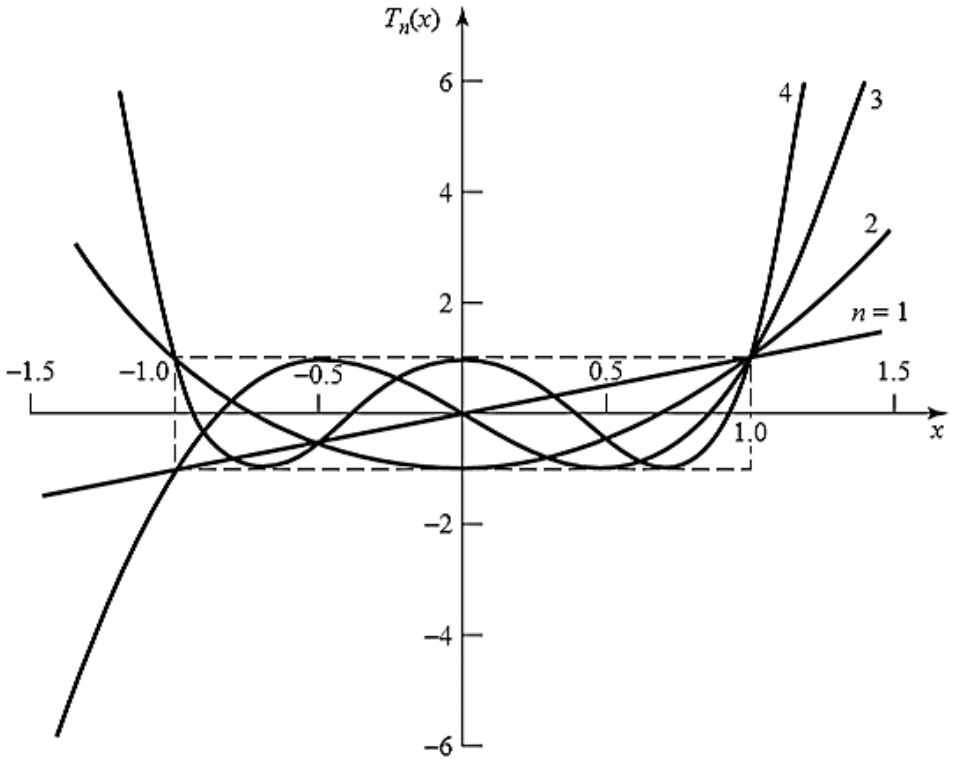

Fig 5.16 - The first four Chebyshev polynomials, $T_n(x)$.

Now let x = cosθ for |x| < 1. Then it can be shown that the Chebyshev polynomials can be expressed as:

$$T_n(\cos\theta) = \cos n\theta,$$

or more generally as

$$T_n(x) = \cos(n\cos^{-1}x) \quad \text{for } |x| < 1, \tag{5.58a}$$

$$T_n(x) = \cosh(n\cosh^{-1}x) \quad \text{for } x > 1. \tag{5.58b}$$

We desire equal ripple for the passband response of the transformer, so it is necessary to map θ_m to x = 1 and $\pi - \theta_m$ to x =−1, where θ_m and $\pi - \theta_m$ are the lower and upper edges of the passband, respectively, as shown in Figure 5.11. This can be accomplished by replacing cosθ in (5.58a) with cosθ/cos θ_m:

$$T_n\left(\frac{\cos\theta}{\cos\theta_m}\right) = T_n(\sec\theta_m\cos\theta) = \cos n\left[\cos^{-1}\left(\frac{\cos\theta}{\cos\theta_m}\right)\right]. \qquad (5.59)$$

Then $|\sec\theta_m \cos\theta| \leq 1$ for $\theta_m < \theta < \pi - \theta_m$, so $|T_n(\sec\theta_m \cos\theta)| \leq 1$ over this same range.

Because $\cos^n \theta$ can be expanded into a sum of terms of the form cos(n−2m)θ, the Chebyshev polynomials of (5.56) can be rewritten in the following useful form:

$$T_1(\sec\theta_m\cos\theta) = \sec\theta_m\cos\theta, \qquad (5.60a)$$

$$T_2(\sec\theta_m\cos\theta) = \sec^2\theta_m(1+\cos 2\theta) - 1, \qquad (5.60b)$$

$$T_3(\sec\theta_m\cos\theta) = \sec^3\theta_m(\cos 3\theta + 3\cos\theta) - 3\sec\theta_m\cos\theta, \qquad (5.60c)$$

$$T_4(\sec\theta_m\cos\theta) = \sec^4\theta_m(\cos 4\theta + 4\cos 2\theta + 3) - 4\sec^2\theta_m(\cos 2\theta + 1) + 1. \qquad (5.60d)$$

These results can be used to design matching transformers with up to four sections, and will also be used in later chapters for the design of directional couplers and filters.

5.2. DESIGN OF CHEBYSHEV TRANSFORMERS

We can now synthesize a Chebyshev equal-ripple passband by making $\Gamma(\theta)$ proportional to $T_N(\sec\theta_m \cos\theta)$, where N is the number of sections in the transformer. Thus, using (5.46), we have

$$\begin{aligned}\Gamma(\theta) &= 2e^{-jN\theta}[\Gamma_0 \cos N\theta + \Gamma_1 \cos(N-2)\theta + \cdots + \Gamma_n \cos(N-2n)\theta + \cdots] \\ &= Ae^{-jN\theta} T_N(\sec\theta_m \cos\theta),\end{aligned} \tag{5.61}$$

where the last term in the series of (5.61) is $(1/2)\Gamma_{N/2}$ for N even and $\Gamma_{(N-1)/2}\cos\theta$ for N odd. As in the binomial transformer case, we can find the constant A by letting $\theta = 0$, corresponding to zero frequency. Thus,

$$\Gamma(0) = \frac{Z_L - Z_0}{Z_L + Z_0} = AT_N(\sec\theta_m),$$

so we have

$$A = \frac{Z_L - Z_0}{Z_L + Z_0} \frac{1}{T_N(\sec\theta_m)}. \tag{5.62}$$

If the maximum allowable reflection coefficient magnitude in the passband is Γ_m, then from (5.61) $\Gamma_m = |A|$ since the maximum value of $T_n(\sec\theta_m \cos\theta)$ in the passband is unity.

Then (5.62) gives

$$T_N(\sec\theta_m) = \frac{1}{\Gamma_m}\left|\frac{Z_L - Z_0}{Z_L + Z_0}\right|,$$

which, after using (5.58b) and the approximations introduced in Section 5.6, allows us to determine θ_m as

$$\sec\theta_m = \cosh\left[\frac{1}{N}\cosh^{-1}\left(\frac{1}{\Gamma_m}\left|\frac{Z_L - Z_0}{Z_L + Z_0}\right|\right)\right]$$
$$\simeq \cosh\left[\frac{1}{N}\cosh^{-1}\left(\left|\frac{\ln Z_L/Z_0}{2\Gamma_m}\right|\right)\right]. \qquad (5.63)$$

Once θm is known, the fractional bandwidth can be calculated from (5.33) as

$$\frac{\Delta f}{f_0} = 2 - \frac{4\theta_m}{\pi}. \qquad (5.64)$$

From (5.61), the Γ_n can be determined using the results of (5.60) to expand $T_N(\sec\theta_m \cos\theta)$ and equating similar terms of the form $\cos(N-2n)\theta$. The characteristic impedances Z_n can be found from (5.43), although, as in the case of the binomial transformer, accuracy can be improved and self-consistency can be achieved by using the approximation that

$$\Gamma_n \simeq \frac{1}{2}\ln\frac{Z_{n+1}}{Z_n}.$$

This procedure will be illustrated in Example 5.7.

The above results are approximate because of the reliance on small-reflection theory but are general enough to design transformers with an arbitrary ripple level, m. Table 5.2 gives exact results [2] for a few specific values of Γ_m for N = 2, 3, and 4 sections; more extensive tables can be found in reference [2].

TABLE 5.2 Chebyshev Transformer Design

	$N = 2$				$N = 3$					
	$\Gamma_m = 0.05$		$\Gamma_m = 0.20$		$\Gamma_m = 0.05$			$\Gamma_m = 0.20$		
Z_L/Z_0	Z_1/Z_0	Z_2/Z_0	Z_1/Z_0	Z_2/Z_0	Z_1/Z_0	Z_2/Z_0	Z_3/Z_0	Z_1/Z_0	Z_2/Z_0	Z_3/Z_0
1.0	1.0000	1.0000	1.0000	1.0000	1.0000	1.0000	1.0000	1.0000	1.0000	1.0000
1.5	1.1347	1.3219	1.2247	1.2247	1.1029	1.2247	1.3601	1.2247	1.2247	1.2247
2.0	1.2193	1.6402	1.3161	1.5197	1.1475	1.4142	1.7429	1.2855	1.4142	1.5558
3.0	1.3494	2.2232	1.4565	2.0598	1.2171	1.7321	2.4649	1.3743	1.7321	2.1829
4.0	1.4500	2.7585	1.5651	2.5558	1.2662	2.0000	3.1591	1.4333	2.0000	2.7908
6.0	1.6047	3.7389	1.7321	3.4641	1.3383	2.4495	4.4833	1.5193	2.4495	3.9492
8.0	1.7244	4.6393	1.8612	4.2983	1.3944	2.8284	5.7372	1.5766	2.8284	5.0742
10.0	1.8233	5.4845	1.9680	5.0813	1.4385	3.1623	6.9517	1.6415	3.1623	6.0920

$N = 4$

	$\Gamma_m = 0.05$				$\Gamma_m = 0.20$			
Z_L/Z_0	Z_1/Z_0	Z_2/Z_0	Z_3/Z_0	Z_4/Z_0	Z_1/Z_0	Z_2/Z_0	Z_3/Z_0	Z_4/Z_0
1.0	1.0000	1.0000	1.0000	1.0000	1.0000	1.0000	1.0000	1.0000
1.5	1.0892	1.1742	1.2775	1.3772	1.2247	1.2247	1.2247	1.2247
2.0	1.1201	1.2979	1.5409	1.7855	1.2727	1.3634	1.4669	1.5715
3.0	1.1586	1.4876	2.0167	2.5893	1.4879	1.5819	1.8965	2.0163
4.0	1.1906	1.6414	2.4369	3.3597	1.3692	1.7490	2.2870	2.9214
6.0	1.2290	1.8773	3.1961	4.8820	1.4415	2.0231	2.9657	4.1623
8.0	1.2583	2.0657	3.8728	6.3578	1.4914	2.2428	3.5670	5.3641
10.0	1.2832	2.2268	4.4907	7.7930	1.5163	2.4210	4.1305	6.5950

6. TAPERED LINES

In the preceding sections we discussed how an arbitrary real load impedance could be matched to a line over a desired bandwidth by using multisection matching transformers. As the number N of discrete transformer sections increases, the step changes in characteristic impedance between the sections become smaller, and the transformer geometry approaches a continuously tapered line. In practice, of course, a matching transformer must be of finite length—often no more than a few sections long. This suggests that, instead of discrete sections, the transformer can be continuously tapered, as

shown in Figure 5.18a. Different passband characteristics can be obtained by using different types of taper.

In this section we will derive an approximate theory, again based on the theory of small reflections, to predict the reflection coefficient response as a function of the impedance taper versus position, Z(z). We will apply these results to a few common types of impedance tapers.

Consider the continuously tapered line of Figure 5.18a as being made up of a number of incremental sections of length z, with an impedance change ΔZ(z) from one

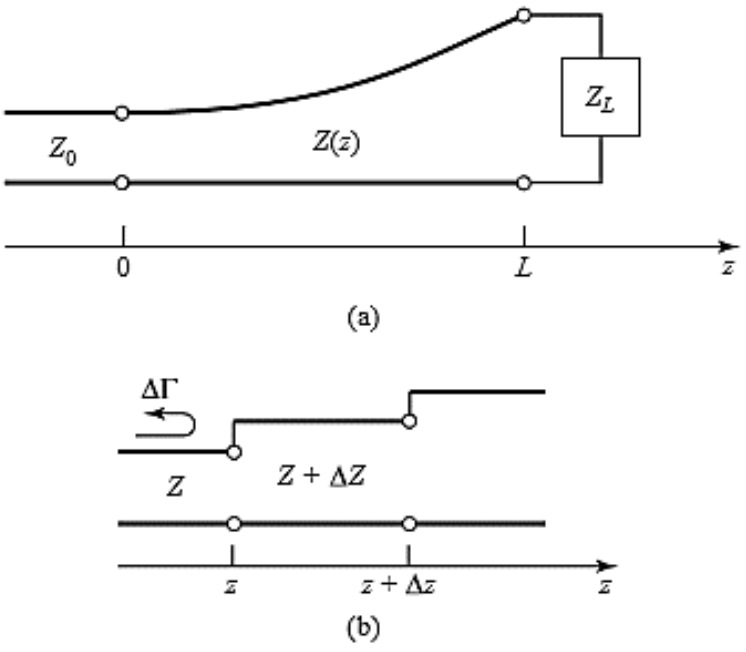

Fig 5.18 - A tapered transmission line matching section and the model for an incremental length of tapered line. **(a)** The tapered transmission line matching section. **(b)** Model for an incremental step change in impedance of the tapered line.

section to the next, as shown in Figure 5.18b. The incremental reflection coefficient from the impedance step at z is given by

$$\Delta\Gamma = \frac{(Z + \Delta Z) - Z}{(Z + \Delta Z) + Z} \simeq \frac{\Delta Z}{2Z}. \tag{5.65}$$

In the limit as $\Delta z \rightarrow 0$ we have an exact differential:

$$d\Gamma = \frac{dZ}{2Z} = \frac{1}{2}\frac{d(\ln Z/Z_0)}{dz}dz, \tag{5.66}$$

Since

$$\frac{d(\ln f(z))}{dz} = \frac{1}{f}\frac{df(z)}{dz}.$$

By using the theory of small reflections, we can find the total reflection coefficient at z = 0 by summing all the partial reflections with their appropriate phase shifts:

$$\Gamma(\theta) = \frac{1}{2}\int_{z=0}^{L} e^{-2j\beta z}\frac{d}{dz}\ln\left(\frac{Z}{Z_0}\right)dz, \tag{5.67}$$

where $\theta = 2\beta\ell$. If Z(z) is known, $\Gamma(\theta)$ can be found as a function of frequency. Alternatively, if $\Gamma(\theta)$ is specified, then in principle Z(z) can be found by inversion. This latter procedure is difficult, and is generally avoided in practice; the reader is referred to references [1] and [4] for further discussion of this topic. Here we will consider three special cases of Z(z) impedance tapers, and evaluate the resulting responses.

6.1. EXPONENTIAL TAPER

Consider first an exponential taper, where

$$Z(z) = Z_0 e^{az} \quad \text{for } 0 < z < L, \tag{5.68}$$

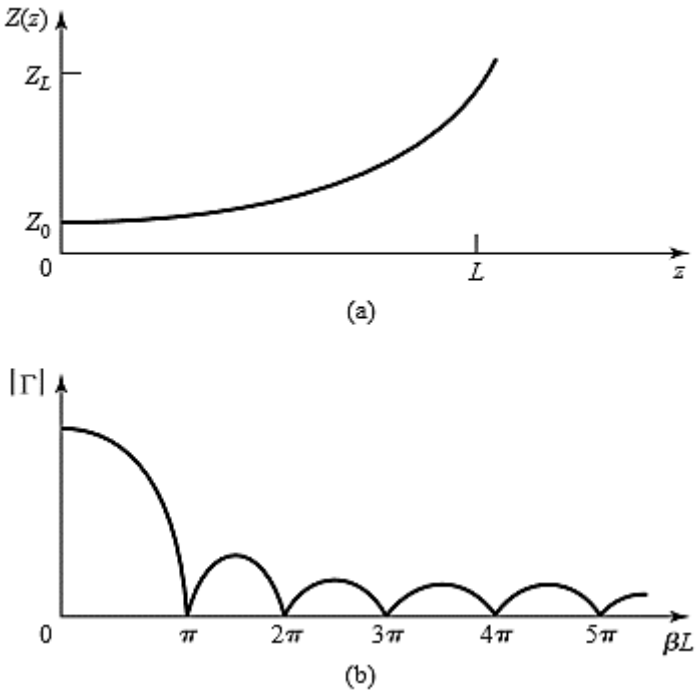

Fig 5.19 - A matching section with an exponential impedance taper. **(a)** Variation of impedance. **(b)** Resulting reflection coefficient magnitude response.

as indicated in Figure 5.19a. At z = 0, Z(0) = Z_0, as desired. At z = L we wish to have Z(L) = $Z_L = Z_0 e^{aL}$, which determines the constant a as

$$a = \frac{1}{L} \ln\left(\frac{Z_L}{Z_0}\right). \tag{5.69}$$

We find Γ(θ) by using (5.68) and (5.69) in (5.67):

$$\begin{aligned} \Gamma &= \frac{1}{2} \int_0^L e^{-2j\beta z} \frac{d}{dz} (\ln e^{az}) dz \\ &= \frac{\ln Z_L/Z_0}{2L} \int_0^L e^{-2j\beta z} dz \\ &= \frac{\ln Z_L/Z_0}{2} e^{-j\beta L} \frac{\sin \beta L}{\beta L}. \end{aligned} \tag{5.70}$$

Observe that this derivation assumes that β, the propagation constant of the tapered line, is not a function of z—an assumption generally valid only for TEM lines.

The magnitude of the reflection coefficient in (5.70) is sketched in Figure 5.19b; note that the peaks in |Γ| decrease with increasing length, as one might expect, and that the length should be greater than λ/2 (βL >π) to minimize the mismatch at low frequencies.

6.2. CHEBYSHEV TAPER

If the number of sections in a Chebyshev transformer is increased indefinitely, with the overall length L kept fixed, we obtain a Chebyshev taper This taper has equal-amplitude minor lobes and is an optimum design in tt sense that it gives the smallest minor-lobe amplitudes for a fixed tap< length, and conversely, for a specified minor-lobe amplitude it has t e shortest length. As such it is a good taper by which to judge how far tapers depart from an optimum design. It has been shown that, in t as the number of sections in a Chebyshev transformer goes to infinity reflection coefficient becomes

$$\Gamma_i = \frac{1}{2} e^{-j\beta L} \ln \bar{Z}_L \frac{\cos L\sqrt{\beta^2 - \beta_0^2}}{\cosh \beta_0 L} \qquad (5.121)$$

where $\beta_{0,,}$ is the value of β at the lower edge of the passband, as illusreted in Fig. 5.55. As increases from zero to β_0, the magnitude ρ_i of Γ_i decreases to a final value of (In Z_L)/(2cosh β_0L), since in cos L $\sqrt{\beta}^2$-β_0^2 = cos L $\sqrt{\beta}_0^2$-β^2 • Beyond this point the function in the numerator is the cosine function that oscillates between ±1 and produces the equal-amplitude minor lobes. The major-lobe to minor-lobe amplitude ratio equals cosβ_0L. Hence, if this is specified so as to keep ρ_i, less than or equal to some maximum value ρ_m in the passband. the taper length L is fixed for a given choice of the frequency of the lower edge of the passband which determines $\beta_{0,}$ We have

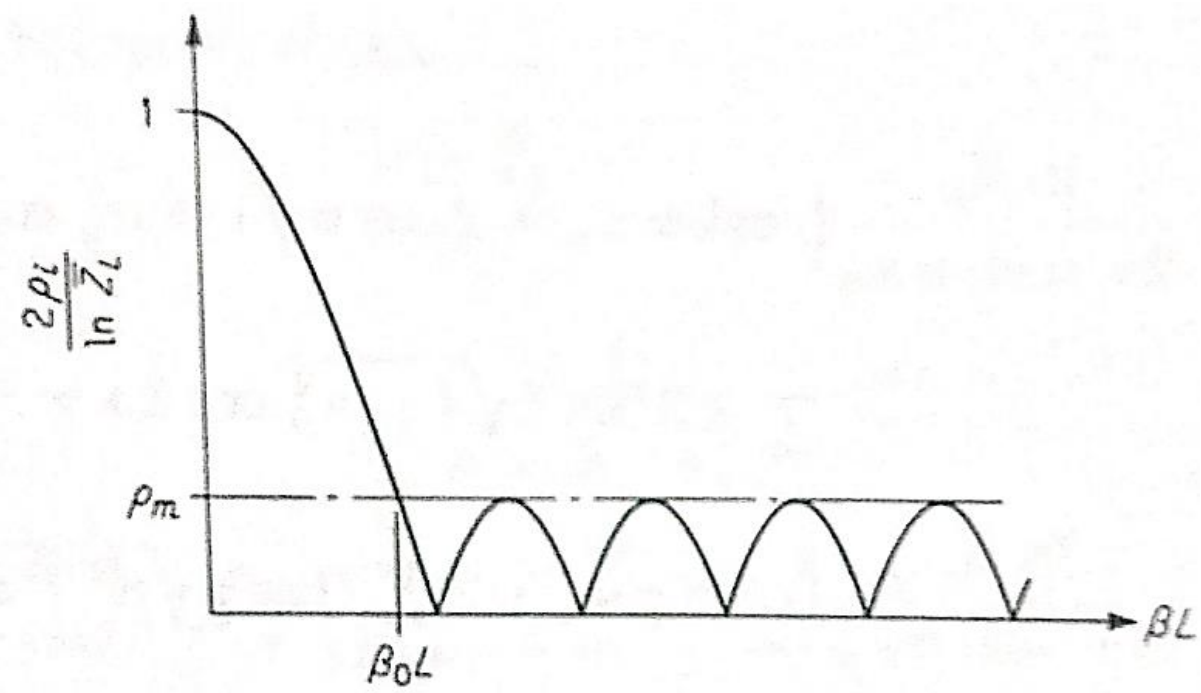

Fig 5.55 - Reflection-coefficient characteristic for a Chebyshev taper.

$$\cosh \beta_0 L = \frac{\ln \bar{Z}_L}{2\rho_m} \qquad (5.122)$$

Conversely, if β_0 and the taper length L are given, the passband tolerance ρ_m is fixed.

The theory given earlier may be used to determine the function g(p) that will produce the reflection coefficient given by (5.121). Introducing the u variable again, we find that the function F(u) is

$$F(u) = (\ln \bar{Z}_L) \frac{\cos \pi \sqrt{u^2 - u_0^2}}{\cosh \pi u_0} \qquad (5.123)$$

where $\pi u = \beta L$, $\pi u_0 = \beta_0 L$. The function $\cos \pi = \sqrt{u^2 - u_0^2}$ can be expressed in infinite-product form as

$$\cos \pi\sqrt{u^2 - u_0^2} = \cosh \pi u_0 \prod_{n=1}^{\infty} \left[1 - \frac{u^2}{u_0^2 + \left(n - \frac{1}{2}\right)^2}\right]$$

and this is the limiting value of the polynomial Q(u) in (5.117) as $N \to \infty$. The sin π u term has been canceled by the infinite product $\Pi_{n=0}^{\infty}$ $(1 - u^2/n^2)$ as in the first example presented on taper synthesis. However, we do not need this product expansion since $2\pi a_n = F(n)$ in any case. From (5.123) we have

$$a_n = a_{-n} = \frac{1}{2\pi} F(n) = \frac{\ln \bar{Z}_L}{2\pi} \frac{\cos \pi\sqrt{n^2 - u_0^2}}{\cosh \pi u_0} \qquad (5.124)$$

Thus

$$\begin{aligned} g(p) &= \frac{\ln \bar{Z}_L}{2\pi \cosh \pi u_0}\left(\cosh \pi u_0 + 2\cos \pi\sqrt{1 - u_0^2} \cos p \right. \\ &\qquad \left. + 2\cos \pi\sqrt{4 - u_0^2} \cos 2p + \cdots\right) \\ &= \frac{\ln \bar{Z}_L}{2\pi \cosh \pi u_0}\left(\cosh \pi u_0 + 2\sum_{n=1}^{\infty} \cos \pi\sqrt{n^2 - u_0^2} \cos np\right) \end{aligned} \qquad (5.125)$$

Integrating with respect to p gives

$$\ln \bar{Z} = \frac{\ln \bar{Z}_L}{2\pi \cosh \pi u_0}\left(p \cosh \pi u_0 + 2\sum_{n=1}^{\infty} \frac{\cos \pi\sqrt{n^2 - u_0^2}}{n} \sin np\right) + C \qquad (5.126)$$

where C is a constant of integration. To render this result more suitable for computation, it is expedient to add and subtract a similar series: i.e.,

$$\ln \bar{Z} = \frac{p \ln \bar{Z}_L}{2\pi} + \frac{\ln \bar{Z}_L}{\pi \cosh u_0 \pi} \sum_{n=1}^{\infty} \frac{\cos n\pi}{n} \sin np$$

$$+ \frac{\ln \bar{Z}_L}{\pi \cosh u_0 \pi} \sum_{n=1}^{\infty} \frac{\cos \pi\sqrt{n^2 - u_0^2} - \cos n\pi}{n} \sin np + C$$

The second series converges rapidly because cos $\pi \sqrt{n^2 - u_0^2}$ approaches cos n π as n becomes large. The first series may be recognized as Fourier sine series for the sawtooth function S(p),

$$S(p) = \begin{cases} -\dfrac{p}{2\pi} \dfrac{\ln \bar{Z}_L}{\cosh \pi u_0} & -\pi < p < \pi \\ 0 & p = \pm\pi \end{cases} \qquad (5.127)$$

and the periodic continuation of this function as illustrated in Fig – 5.56

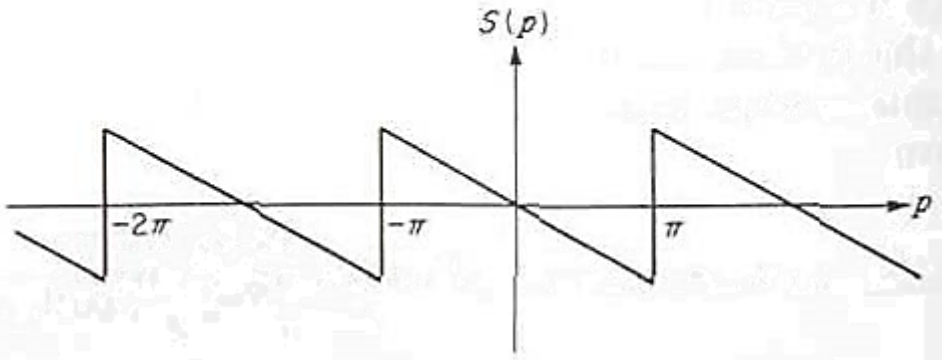

Fig 5.56 – Sawtooth function

Hence we obtain

$$\ln \bar{Z} = \frac{p \ln \bar{Z}_L}{2\pi} + \frac{\ln \bar{Z}_L}{\pi \cosh u_0 \pi} \sum_{n=1}^{\infty} \frac{\cos n\pi}{n} \sin np$$

$$+ \frac{\ln \bar{Z}_L}{\pi \cosh u_0 \pi} \sum_{n=1}^{\infty} \frac{\cos \pi\sqrt{n^2 - u_0^2} - \cos n\pi}{n} \sin np + C$$

At p = π, we have In $\overline{Z}$ = In $\overline{Z}_L$, and since S(p) and sin np are zero at this point, C + $\frac{1}{2}$ In $\overline{Z}_L$ = In $\overline{Z}_L$ or C + $\frac{1}{2}$ In $\overline{Z}_L$, Our final result is

$$\ln \bar{Z} = \left(\frac{p}{2\pi} + \frac{1}{2} - \frac{p}{2\pi \cosh \pi u_0} \right) \ln \bar{Z}_L + \frac{\ln \bar{Z}_L}{\pi \cosh \pi u_0} \sum_{n=1}^{\infty} \frac{\cos \pi \sqrt{n^2 - u_0^2} - \cos n\pi}{n} \sin np \quad (5.128)$$

for -π <p < π. An interesting feature of the above result is that In $\overline{Z}$ changes in a stepwise fashion from 0 to (In $\overline{Z}$;)/(2cosh π u_0) as p changes from -π - ε to -π + ε, where ε « 1. Likewise, at the other end of the taper, In $\overline{Z}$ changes abruptly from a value In $\overline{Z}_L$ - (In $\overline{Z}_L$)/(2cosh πu_0) to In Z_L; as the point p = π is reached. This means that the optimum taper has a step change in impedance at each end. The physical basis for this is readily understood by noting that when the frequency is very high, so that the taper is many wavelengths long, the reflection from the smooth part of the taper vanishes. Thus, in order still to maintain equal-amplitude minor lobes, the two-step changes in impedance must be provided to give a reflection coefficient

$$\rho_i = \frac{\ln \bar{Z}_L}{2} \frac{\cos \beta L}{\cosh \beta_0 L} \qquad \text{for } \beta \gg \beta_0$$

As an indication of the superiority of the Chebyshev taper, computations show that it is 27 percent shorter than the taper with d(ln $\overline{Z}$)/dz a triangular function, for the same passband tolerance and lower cutoff frequency. If the tapers are made the same length, the Chebyshev taper provides a major- to minor-lobe ratio of 84 as compared with 21 for the taper with a triangular distribution.

7. REFERENCES

[1] R. E. Collin, Foundations for Microwave Engineering, 2nd edition, McGraw-Hill, New York, 1992.

[2] G. L. Matthaei, L. Young, and E. M. T. Jones, Microwave Filters, Impedance-Matching Networks, and Coupling Structures, Artech House Books, Dedham, Mass. 1980.

[3] P. Bhartia and I. J. Bahl, Millimeter Wave Engineering and Applications, Wiley Interscience, New York, 1984.

[4] R. E. Collin, "The Optimum Tapered Transmission Line Matching Section," Proceedings of the IRE, vol. 44, pp. 539–548, April 1956.

[5] R. W. Klopfenstein, "A Transmission Line Taper of Improved Design," Proceedings of the IRE, vol. 44, pp. 31–15, January 1956.

[6] M. A. Grossberg, "Extremely Rapid Computation of the Klopfenstein Impedance Taper," Proceedings of the IEEE, vol. 56, pp. 1629–1630, September 1968.

[7] H. W. Bode, Network Analysis and Feedback Amplifier Design, Van Nostrand, New York, 1945.

[8] R. M. Fano, "Theoretical Limitations on the Broad-Band Matching of Arbitrary Impedances," Journal of the Franklin Institute, vol. 249, pp. 57–83, January 1950, and pp. 139–154, February 1950.

Chapter 5

DESIGN PROCEDURE

The above analysis is summarized below in convenient form for use in designing a matching taper. Let the characteristic impedance of the output line, normalized with respect to the impedance of the input line, be Z_2. Let the maximum tolerable value of the reflection coefficient in the pass band be ρ_m, The major to minor lobe ratio η is given by cosh ,$\beta_0 L$ where

$$\cosh \beta_0 L = \frac{\ln Z_2}{2\rho_m} \qquad (29)$$

This relation determines the ideal cutoff value $\beta_0 L$. The practical cutoff value $\beta_0 L$ is equal to $\sigma\beta_0 L$ where

$$\sigma = \frac{\bar{n}\pi}{\sqrt{\beta_0^2 L^2 + (\bar{n} - \frac{1}{2})^2 \pi^2}} \qquad (30)$$

and $\underline{n}$ must be chosen greater than

$$\frac{2\beta_0^2 L^2}{\pi^2} + \frac{1}{2} \cdot$$

For a cutoff wavelength of λ_c, the physical length of taper required is

$$L = \frac{\sigma\lambda_c}{2\pi} \operatorname{arc\,cosh} \frac{\ln Z_2}{2\rho_m} \cdot \qquad (31)$$

The variation in taper impedance required is

$$Z(y) = \exp\left(\sum_0^{\bar{n}-1} \frac{\epsilon_{0m}}{m\pi} F(m) \sin \frac{2m\pi}{L} y + \frac{F(0)}{2} \right) \qquad (32)$$

Where

$$F(m) = -\ln Z_2 \frac{\cos m\pi}{2} \cdot \frac{\prod_{n=1}^{\bar{n}-1}\left(1 - \frac{m^2\pi^2}{\sigma^2\left[\beta_0{}^2L^2 + (n-\frac{1}{2})^2\pi^2\right]}\right)}{\prod_{n=1\cdot n\neq m}^{\bar{n}-1}\left(1 - \frac{m^2}{n^2}\right)} \quad (33)$$

and F(0) =ln Z_2. The reflection coefficient is given by (28). The design is somewhat conservative since the major to minor lobe ratio is slightly greater than η.

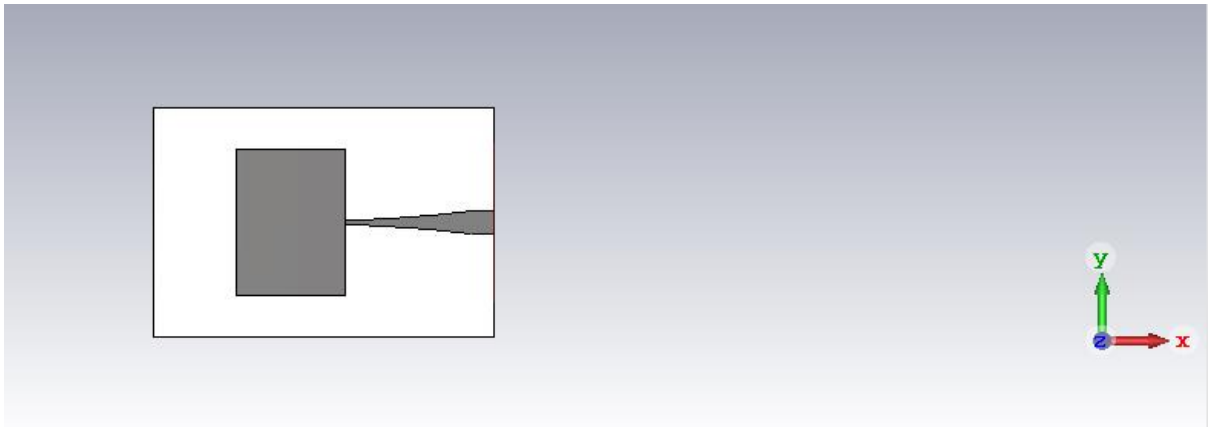

Fig 1 – Designed by Simulation Software

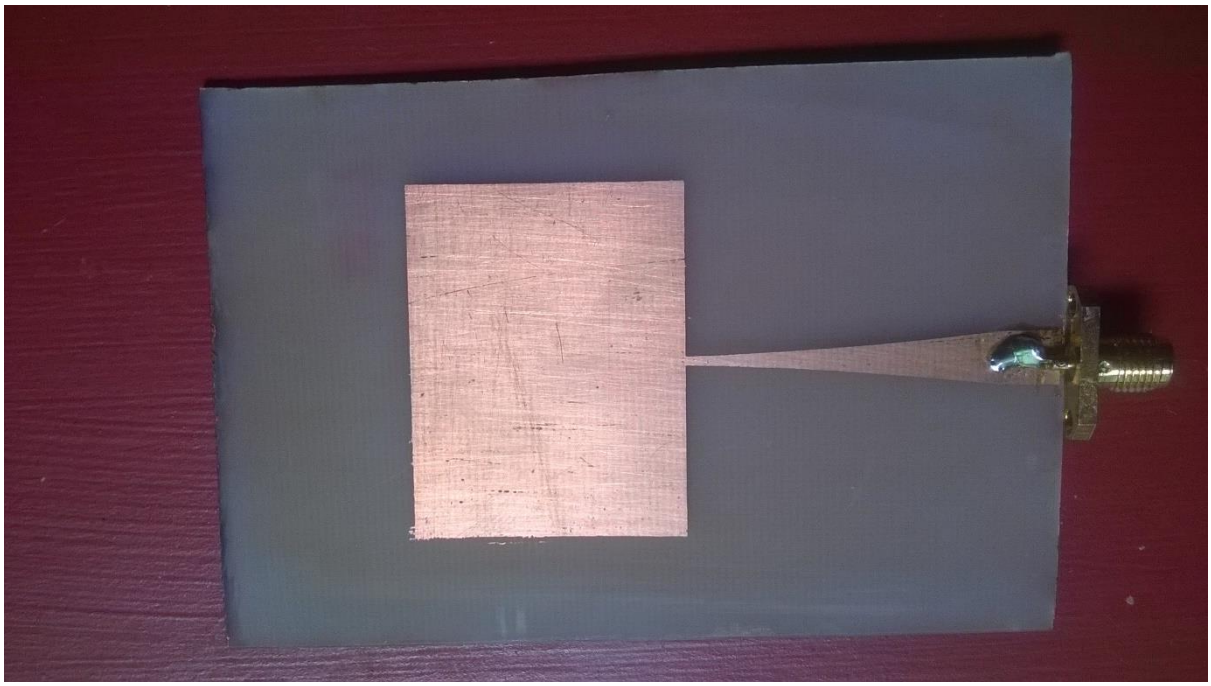

Fig 1.1 – Designed by Fabrication in Lab

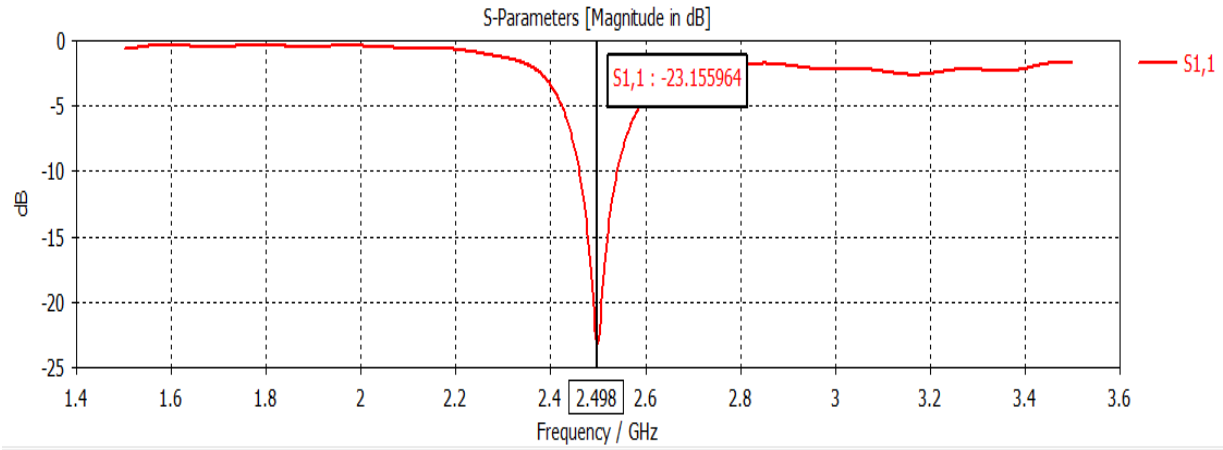

Fig 2 – Simulated S_{11} (in dB) vs Frequency (in GHz)

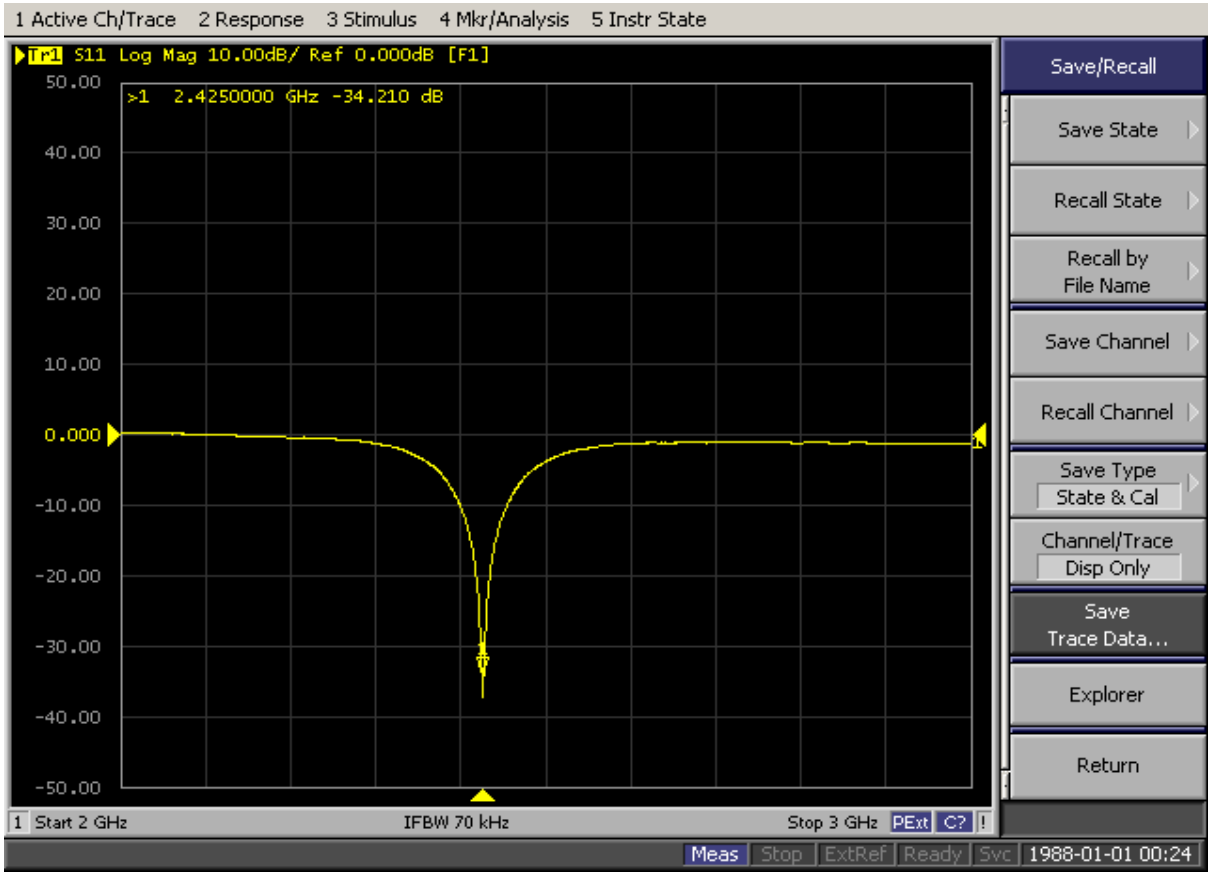

Fig 2.1 – Calculated S_{11} plot from Vector Spectrum Analyzer in practical experiment

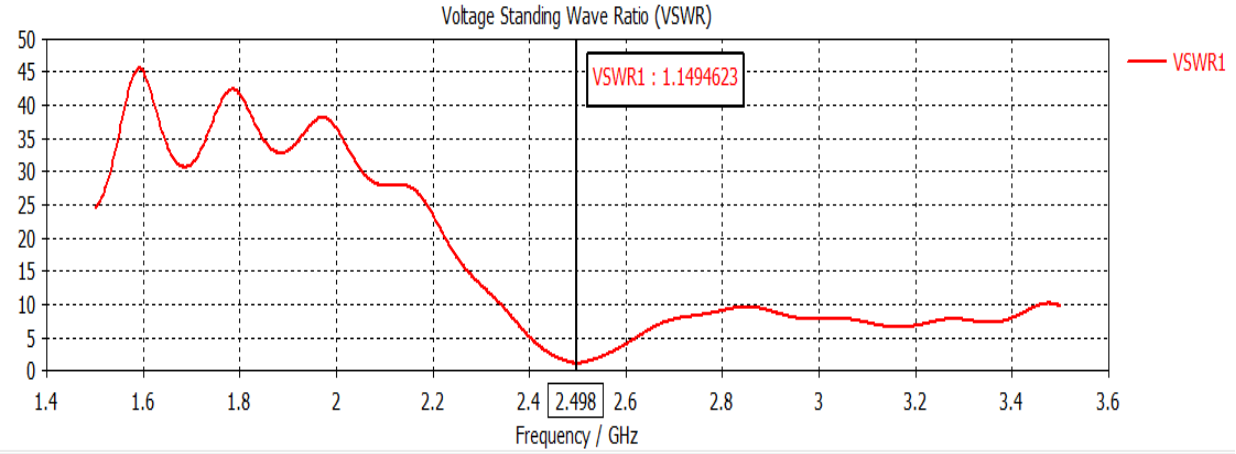

Fig 3 - VSWR by Simulation Software

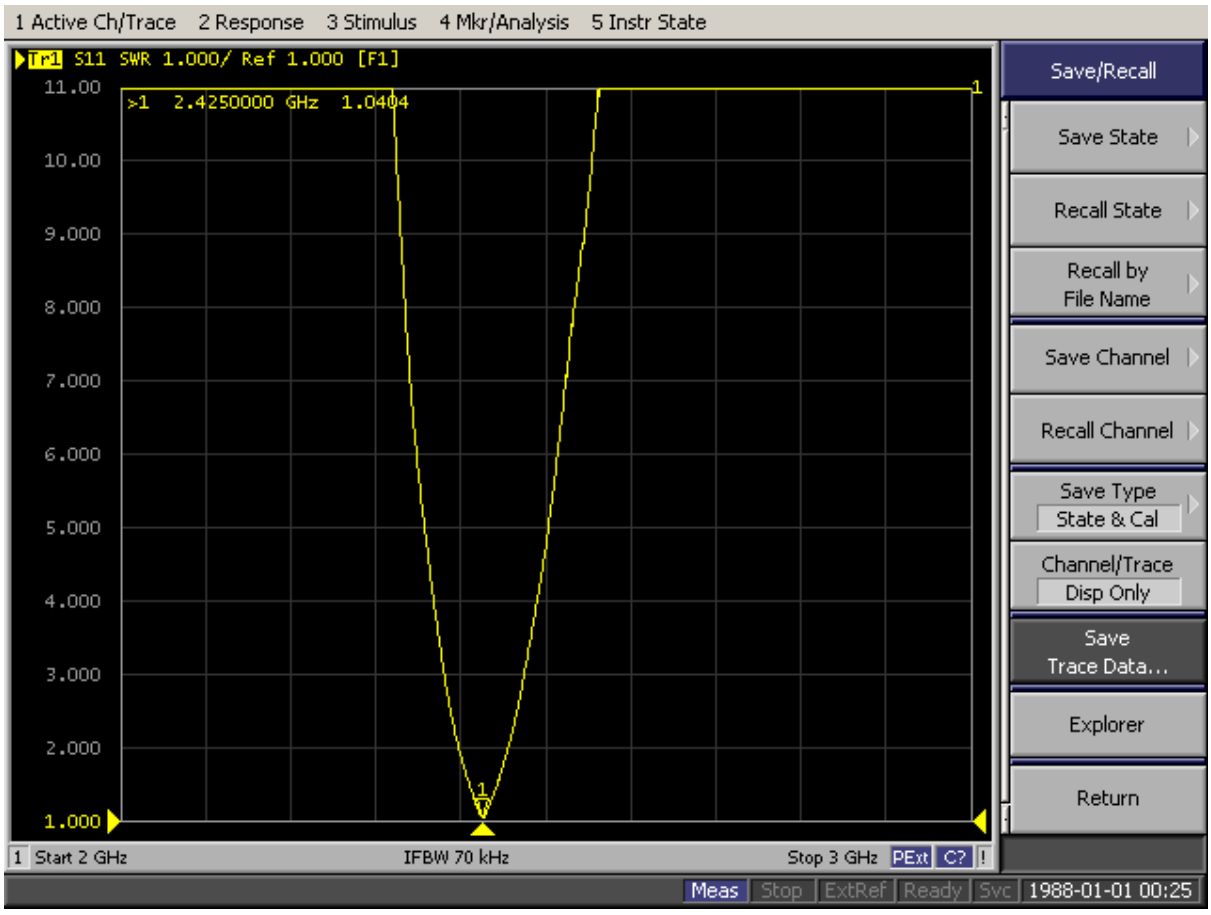

Fig 3.1 – VSWR by Voltage Spectrum Analyzer

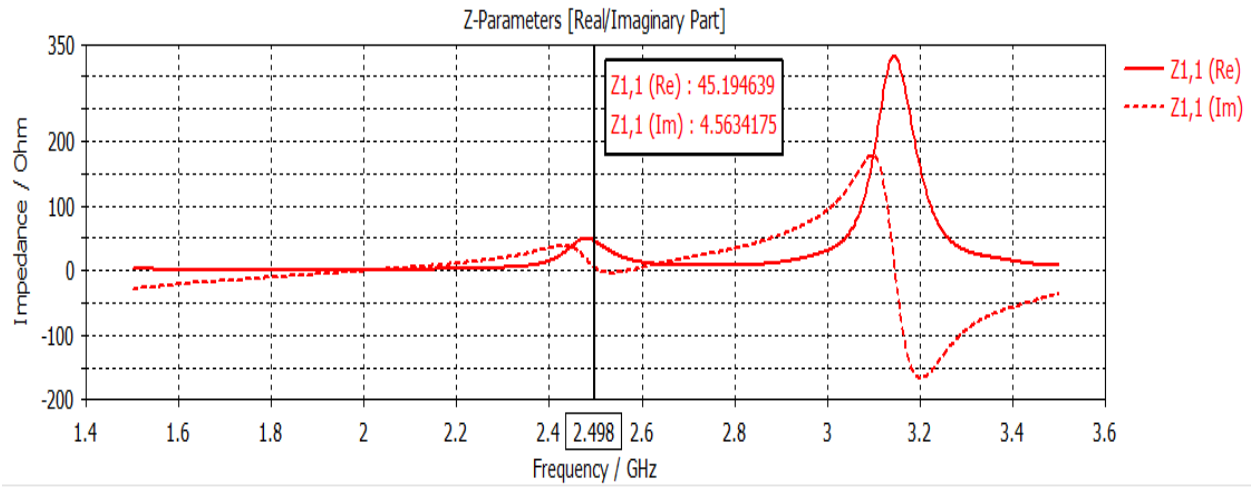

Fig 4 – Z_{11} Parameter by Simulation Software

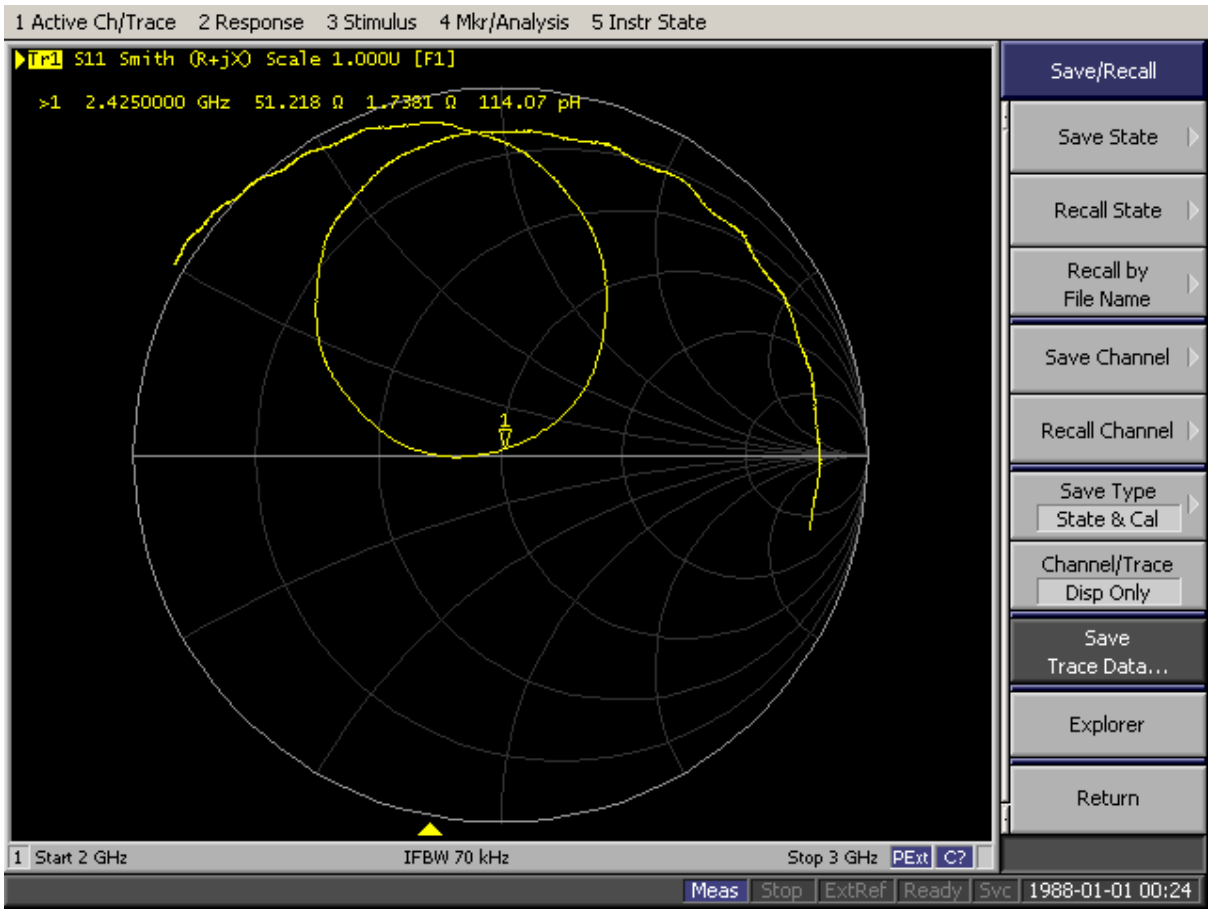

Fig 4.1 – Smith Chart

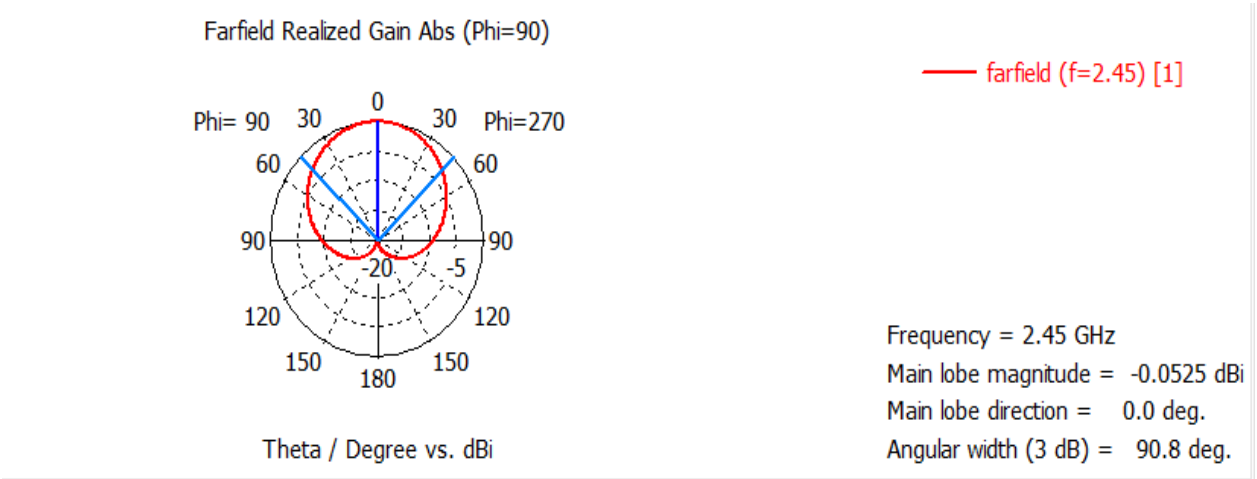

Fig 5 – Radiation Pattern by Simulation Software

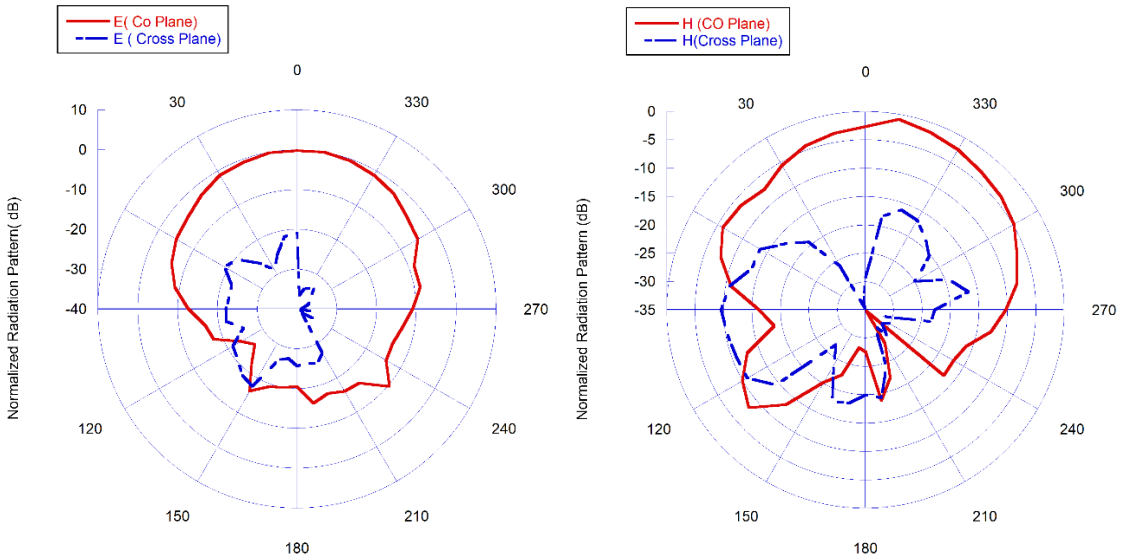

Fig 5.1 – Measured normalized E - plane and H - plane

(Here we can ovserve that, as we have considered the far-field values at an interval of 10 degree, we have seen the measured radiation pattern is somewhat coarse and is somewhat different from that we simulated)

Chapter 6

MOTIVATION AND GOALS

Microstrip Antenna suffers from low bandwidth (<5%) and low gain predominantly owing to promulgation of surface waves. Surface wave promulgation is severe problematic in microstrip antenna. Surface wave diminishes antenna efficiency and gain, limits bandwidth, surges end-fire radiations, escalates cross-polarization and limits the useful frequency range of microstrip antennas. Microstrip Patch Antenna (MPA) has a conducting patch of low surface impedance printed on a grounded dielectric substrate. The ground plane supports propagating TM surface waves. These waves travel along the surface that causes undesirable end–fire radiations. The image current is out of phase with antenna current thereby causes fading of the radiation pattern.

Mutual coupling happens together in surface waves (the primary mode TM0 requires zero cutoff frequency and is permanently present but influence is more noticeable in E-plane rather than H-plane) and in expressions of space waves. The elements initiating mutual coupling are substrate dielectric strength, substrate thickness and space among individual patches. Surface waves turn out to be reasonably greater than space waves when high dielectric and high thickness of substrate is used.

In addition in many of the stated applications of MPA there would be a multi-frequency operations requirement. So the improvement of the bandwidth and the attainment of multi frequency setup are major tasks for the MPA.

Considerable research has been done in the use of UWB systems since the Federal communication commission (FCC) unconfined the frequency range 3.1-10.6 GHz. It is because of their small power intake, less budget, accurate locating and encouraging contender for short-range high-speed indoor information transmission. Circular monopoles are a good example for UWB uses owing to their advantages like simplicity of production, satisfactory radiation characteristics and huge impedance bandwidth. Nevertheless, narrowband arrangements also function in this frequency like worldwide interoperability for microwave access WiMAX band (3.3-3.8 GHz), wireless local area network WLAN band (5.15-5.825 GHz) and X-Band downlink satellite communication band (7.1-7.9 GHz). To avoid any intervention from these systems it is required to design UWB antenna with band notch features.

Multiple-input–multiple-output (MIMO)/Diversity antennas based communication systems have multiple antennas that are used at transmitter and receiver terminals to improve the data rate in multipath signal propagation. The signal strength can be improved by sending data bits with multiple antennas at the transmitter and data bits are reassembled at the receiver. When MIMO systems are used for compact portable devices, high electromagnetic coupling between antennas affect the system performance considerably.

This thesis aims to contribute towards research of Electromagnetic Band Gap (EBG) structures integrated with microstrip antenna. A survey on EBG structures, its properties, bandwidth enhancement due to suppression of surface waves and reduction of mutual coupling with EBG structures is reported. Lastly, development of notched UWB with uniplanar and mushroom EBG structures which is antenna design independent approach has been carried out.

Chapter 7

CONCLUSION

In this project we design a rectangular patch antenna which is feed with Transfer coupled tapered line and is operated at 2.45 GHz. This antenna can be easily fabricated as the thickness of substrate and small size. Considering the graph which we get after simulation of microstrip antenna can be stated that the designed antenna is characterized by good electrical parameter. The shape of the radiation pattern is approximately matched with theoretical assumption. The design antenna exhibits a good impedance matching of approximately 50 Ohms at the center frequency. Microstrip antenna are widely used in the construction of the modern antenna which is used in radar, WIFI and in many communication systems.

REFERENCES

[1] 1. C.A. Balanis, Antenna Theory Analysis & Design, 2ndEdition, John Wiley & Sons, New York, 1997.

[2] K.R. Carver and J.W. Mink, "Microstrip AntennaTechnology", IEEE Trans.Antenna Propagation, Vol. AP –29 , No. 1, pp.2 –24, January 1981.

[3] I.J.Bahl and P. Bhartia , Microstrip Antenna, Washington 1980Nazifa Mariam, " Comparison between inset and coaxial feed excitation technique of microstrip antenna",

[4] Proceedings of Conference on information science, technology and management (CISTM2007) Hyderabad, India, July 16-18, 2007

[5] W.F. Richards, Y.T Lo, and D.D Harrison, " An Improved theory of Microstrip Antenna with Applications", IEEE Trans. Antenna Propagation, Vol. AP–29 , No. 1, pp. 38 –46, January 1981

[6] 6. W.L. Stutzman, G.A. Thiele, Antenna Theory and design, John Wiley & Sons, 2nd Ed., New York, 1998.

[7] E. H. Miller, "A note on reflector arrays (Periodical style—Accepted for publication)," IEEE Trans. Antennas Propagat., to be published

List of Figures:

List of Tables: